

# Synchronization of chaotic systems: Transverse stability of trajectories in invariant manifolds

Reggie Brown and Nikolai F. Rulkov

*Institute for Nonlinear Science, University of California, San Diego, La Jolla, California 92093-0402*

(Received 19 August 1996; accepted for publication 22 April 1997)

We examine synchronization of identical chaotic systems coupled in a drive/response manner. A rigorous criterion is presented which, if satisfied, guarantees that synchronization to the driving trajectory is linearly stable to perturbations. An easy to use approximate criterion for estimating linear stability is also presented. One major advantage of these criteria is that, for simple systems, many of the calculations needed to implement them can be performed analytically. Geometrical interpretations of the criterion are discussed, as well as how they may be used to investigate synchronization between mutual coupled systems and the stability of invariant manifolds within a dynamical system. Finally, the relationship between our criterion and results from control theory are discussed. Analytical and numerical results from tests of these criteria on four different dynamical systems are presented. © 1997 American Institute of Physics. [S1054-1500(97)00303-0]

**If several identical dynamical systems travel the same phase space trajectory at the same time, then they are said to be synchronized. Examples of this type of behavior go back at least as far as Huygens. Surprisingly, this type of behavior has also been observed for chaotic systems. If the systems are chaotic, then they must be coupled together in some fashion. A typical procedure for determining a type of coupling that produces synchronous motion is to try different couplings until one of them works. This paper presents a rigorous criterion and approximate version that, if satisfied, guarantees linearly stable synchronous motion for the systems. To use the criterion one only needs the equations of motion and the trajectory one wants the systems to follow. The paper also presents a step by step procedure that will allow one to design couplings that satisfy these criteria. Since the procedure does not use trial and error, and (for simple systems) many of the steps can be performed analytically, it is an improvement over current practice.**

## I. INTRODUCTION

Since Fujisaka and Yamada's 1983 paper on synchronized motion in coupled chaotic systems many researchers have discussed the stability of this type of motion.<sup>1</sup> Rather than attempt to reference a complete list of papers on this topic we refer the interested reader to Refs. 2–9. (These papers have extensive bibliographies and represent a reasonable introduction to the literature.) The discussion in this paper will center around the type of synchronization discussed by most of these authors. Namely, two or more *identical* chaotic systems, coupled in a drive/response manner, which exhibit motion that is chaotic and *identical* in time. (Although the dynamical systems we examine are chaotic our results are applicable to nonlinear systems that exhibit other types of motion.)

The central question addressed in this paper is: "Given two arbitrary identical dynamical systems how can one de-

sign a physically available coupling scheme that is guaranteed to produce stable synchronized motion?" Despite the large amount of effort devoted to this issue there are relatively few rigorous results. In most cases rigorous results are obtained using Lyapunov functions.<sup>10–13</sup> Unfortunately, this method is not regular since, in practice, it can only be applied to particular examples; i.e., given an arbitrary dynamical system it is not clear how one can derive a coupling scheme and/or a Lyapunov function which guarantees stable synchronous motion.

Another rigorous approach is that of Ashwin *et al.*<sup>14</sup> In a series of papers they presented results that are related to the central question. In their work the measure (equivalently, the trajectory) used to describe the dynamics of the system is of central importance. To apply the approach one must show that all normal Lyapunov exponents are negative for all measures of the dynamics. Unfortunately, it is well known that Lyapunov exponents can be difficult to calculate. Non-rigorous results that employ Lyapunov exponents to determine the stability of measures to perturbations have also appeared in the literature.<sup>7,8,15–17</sup>

A third rigorous approach by Walker and Mees has recently appeared.<sup>18</sup> They used the method of Lyapunov to develop a sufficient condition for stable synchronization. Their condition relates eigenvalues of the linear part of the vector field to the Jacobian of the nonlinear part. The analysis in this paper also differs from that in other papers because they interpret synchronization as an observer problem.

Finally, there are a few special cases where, due to the coupling between the nonlinear systems, rigorous analysis of the stability of synchronization is straightforward. One case is when the coupling transforms the driven system into a stable homogeneous linear system with time dependent external forcing (see Ref. 19). A second is when the coupling between all of the variables is diagonal.<sup>1,7</sup> In many practical cases these types of coupling can't be achieved.

The approach advocated in this paper is like that of Ashwin *et al.* in that it emphasizes the role of individual trajec-

tories within the dynamics of the system. However, we do not explicitly use Lyapunov exponents or Lyapunov functions to examine the linear stability of synchronous motion. It is also like the paper by Walker and Mees in that their stability condition and design concepts are similar to the one we develop below. The issue of design has also been addressed by Peng *et al.*<sup>17</sup>

We have two major results. The first is a rigorously derived criterion which, if satisfied, *guarantees* that the coupling scheme will yield linearly stable synchronous motion on the driving trajectory. The second result is a simple, “quick and dirty” criterion that can be used to estimate the coupling needed for linear stability. This second criterion is easy to implement and can be used to quickly examine a large range of coupling schemes and strengths. For both cases, linear stability is with respect to perturbations that are transverse to the synchronization manifold. (Of course, because our results are obtained from a linearization they can not fully address the complications that arise when nonlinear effects are incorporated. Some of these difficulties are discussed in Section V.)

References 8, 14, and 20–22, and the results presented below, indicate that the stability of the synchronization manifold depends on the measure used to describe the dynamics on the manifold. If the synchronization manifold contains a set of chaotic trajectories, then there are an infinite number of possible measures for the dynamics on the manifold. Under these circumstances a practical answer to the question of the stability of the synchronization manifold can be quite complicated. For example, the manifold may be linearly unstable when using a measure confined to one periodic orbit on the manifold (a Dirac measure<sup>14</sup>) and linearly stable on a measure confined to a different periodic orbit. At the end of the next section we discuss relevant results that may allow one to overcome this difficulty.

We close this section with an outline of the remainder of this paper. In Sections II and III we derive criteria that indicate when synchronization between drive and response systems will occur. The results in Section II are rigorous while those in Section III are approximations. Section IV presents results from analytic examinations and numerical experiments we have conducted on the Rössler, Lorenz, and Ott–Sommerer systems. In Section V we summarize our results and discuss how nonlinear effects impact our results. In Appendix A we discuss how our results apply to other systems (in this appendix we examine a system of equations that come about when considering chaotic masking for private communications). In Appendix B we present geometric interpretations of the manifolds that arise in our discussion, while in Appendix C we discuss a geometrical interpretation of the theoretical results. In Appendix D we discuss the relationship between our results and control theory, while Appendix E is devoted to an alternative analysis of our criterion and an additional examination of the Lorenz system.

## II. THEORY PART I: RIGOROUS RESULTS

This section presents rigorous results regarding linear stability of trajectories on the invariant manifold associated

with synchronous motion. (Here, and for the remainder of this paper, when we say synchronization to a trajectory is linearly stable we mean it is linearly stable with respect to perturbations that are transverse to the part of the synchronization manifold defined by the driving trajectory.)

We will explicitly examine one type of drive/response coupling for identical systems that have chaotic uncoupled dynamics.<sup>23–25</sup> Assume the dynamics of the driving system is given by

$$\frac{d\mathbf{x}}{dt} = \mathbf{F}(\mathbf{x}; t), \quad (1)$$

where  $\mathbf{x} \in \mathbb{R}^d$ . In the presence of coupling the dynamics of the response system becomes

$$\frac{d\mathbf{y}}{dt} = \mathbf{F}(\mathbf{y}; t) + \mathbf{E}(\mathbf{x} - \mathbf{y}), \quad (2)$$

where  $\mathbf{E}$  is a vector function of its argument and represents coupling between the systems. We assume  $\mathbf{E}(\mathbf{0}) = \mathbf{0}$ , hence synchronization occurs on the invariant manifold given by  $\mathbf{x} = \mathbf{y}$ . Obviously, if the coupling strength is below some critical threshold, then synchronization will not occur. In addition, for some  $\mathbf{F}$ 's and choices of  $\mathbf{E}$ , synchronous motion only occurs within a finite range of coupling strengths. For these situations, if the coupling strength is too small or too large, then synchronization will not occur. Finally, for some  $\mathbf{F}$ 's and choices of  $\mathbf{E}$  synchronization will never occur.

Since we are interested in deviations of  $\mathbf{y}$  from  $\mathbf{x}$  we use Eqs. (1) and (2) to obtain the following linearized equation of motion for  $\mathbf{w} \equiv \mathbf{y} - \mathbf{x}$  (motion transverse to the synchronization manifold):

$$\frac{d\mathbf{w}}{dt} = [\mathbf{DF}(\mathbf{x}; t) - \mathbf{DE}(\mathbf{0})]\mathbf{w}. \quad (3)$$

In this equation  $\mathbf{DF}(\mathbf{x}; t)$  is the Jacobian of  $\mathbf{F}$  evaluated at  $\mathbf{x}$  at time  $t$ , and  $\mathbf{DE}(\mathbf{0})$  is the Jacobian of  $\mathbf{E}$  evaluated at  $\mathbf{w} = \mathbf{0}$ . The synchronization manifold is linearly stable if

$$\lim_{t \rightarrow \infty} \|\mathbf{w}(t)\| = \lim_{t \rightarrow \infty} \|\mathbf{y}(t) - \mathbf{x}(t)\| = 0$$

for all possible driving trajectories,  $\mathbf{x}(t)$ . [Notice that a stability analysis of synchronized chaos needs to consider only the trajectories,  $\mathbf{x}(t)$ , that belong to the chaotic attractor of the driving system.] We begin determining the behavior of  $\mathbf{w}(t)$  in this limit by dividing  $\mathbf{DF}(\mathbf{x}; t) - \mathbf{DE}(\mathbf{0})$  into a time independent part,  $\mathbf{A}$ , and an explicitly time dependent part,  $\mathbf{B}(\mathbf{x}; t)$ ,

$$\mathbf{DF}(\mathbf{x}; t) - \mathbf{DE}(\mathbf{0}) \equiv \mathbf{A} + \mathbf{B}(\mathbf{x}; t). \quad (4)$$

This decomposition is not unique since we are free to add constant terms to  $\mathbf{A}$  provided we are willing to subtract the same term from  $\mathbf{B}$ . This freedom will be resolved later when an explicit decomposition is determined. For now the reader is asked to accept Eq. (4) as a formal decomposition.

Denote, and order, the eigenvalues of  $\mathbf{A}$  by  $\Re[\Lambda_1] \geq \Re[\Lambda_2] \geq \dots \geq \Re[\Lambda_d]$ , where  $\Re[\Lambda]$  is the real part of the eigenvalue  $\Lambda$ . Associated with the eigenvalues are eigenvectors denoted by  $\hat{\mathbf{e}}_1, \hat{\mathbf{e}}_2, \dots, \hat{\mathbf{e}}_d$ . Next, assume  $\mathbf{A}$  can be diagonalized by  $\mathbf{P} = [\hat{\mathbf{e}}_1 \hat{\mathbf{e}}_2 \dots \hat{\mathbf{e}}_d]$ . Thus,  $\mathbf{D} = \mathbf{P}^{-1} \mathbf{A} \mathbf{P}$  is a diagonal matrix. Rewriting Eq. (4) in terms of the coordinate system defined by the eigenvectors of  $\mathbf{A}$  yields

$$\frac{d\mathbf{z}}{dt} = [\mathbf{D} + \mathbf{K}(\mathbf{x}; t)] \mathbf{z},$$

where  $\mathbf{z} = \mathbf{P}^{-1} \mathbf{w}$  and  $\mathbf{K} = \mathbf{P}^{-1} \mathbf{B} \mathbf{P}$ . Next, define the time evolution operator  $\mathbf{U}(t, t_0) = \exp[\mathbf{D}(t - t_0)]$  and use the method of variation of constants to rewrite the linearized equation of motion as the following integral equation:<sup>26</sup>

$$\mathbf{z}(t) = \mathbf{U}(t, t_0) \mathbf{z}(t_0) + \int_{t_0}^t \mathbf{U}(t, s) \mathbf{K}(s) \mathbf{z}(s) ds, \quad (5)$$

where  $\mathbf{K}(s) \equiv \mathbf{K}[\mathbf{x}(s); s]$  denotes  $\mathbf{K}$  evaluated along the driving trajectory.

The linear stability of synchronization to the driving trajectory,  $\mathbf{x}(t)$ , is determined by the behavior of  $\|\mathbf{z}(t)\|$  in the  $t \rightarrow \infty$  limit. To determine this behavior the remainder of the calculations in this section closely follow those of Chapter 6 in Ref. 26. Begin by using norms to obtain the following inequality:<sup>27</sup>

$$\|\mathbf{z}(t)\| \leq \|\mathbf{U}(t, t_0)\| \|\mathbf{z}(t_0)\| + \int_{t_0}^t \|\mathbf{U}(t, s)\| \|\mathbf{K}(s)\| \|\mathbf{z}(s)\| ds.$$

It is known that if  $\Re[\Lambda_1] < 0$ , then  $\|\mathbf{U}(t, t_0)\| \leq C \exp[-\mu(t - t_0)]$  for appropriate choices of  $C$  and  $\mu$ . Inserting this into the inequality and applying Gronwall's Theorem<sup>26</sup> yields

$$\|\mathbf{z}(t)\| \leq C \|\mathbf{z}(t_0)\| \exp\left[\int_{t_0}^t (C \|\mathbf{K}(s)\| - \mu) ds\right].$$

Hence, a sufficient condition for linearly stable synchronization is

$$\mu > \lim_{t \rightarrow \infty} \frac{C}{t - t_0} \int_{t_0}^t \|\mathbf{K}(s)\| ds, \quad (6)$$

which depends on  $C$ ,  $\mu$ ,  $\|\mathbf{K}\|$ , and the measure of the driving signal,  $\mathbf{x}(t)$ .

The constants  $C$  and  $\mu$  depend explicitly on the choice of matrix norm. A common choice is the Frobenius norm<sup>27</sup>

$$\|\mathbf{M}\| \equiv [\text{Tr}(\mathbf{M}^\dagger \mathbf{M})]^{1/2} = \left[ \sum_{\alpha, \beta=1}^d |M_{\alpha\beta}|^2 \right]^{1/2},$$

where the  $\dagger$  denotes Hermitian conjugate and Greek subscripts denote elements of matrices ( $M_{\alpha\beta}$  is the  $\alpha\beta$  element of the matrix  $\mathbf{M}$ ). Applying this norm to  $\mathbf{U}(t, t_0)$  and using the rank ordering of the  $\Lambda$ 's implies that, in the large  $t$  limit,  $\|\mathbf{U}(t, t_0)\| \approx \exp[\Re[\Lambda_1](t - t_0)]$ , an approximation that becomes exact in the  $t \rightarrow \infty$  limit. Therefore, in this limit,  $C = 1$  and  $\mu = -\Re[\Lambda_1]$ .

Inserting these results into Eq. (6) indicates that the sufficient condition for linear stability of synchronization along the driving trajectory  $\mathbf{x}(t)$  is

$$-\Re[\Lambda_1] > \lim_{t \rightarrow \infty} \frac{1}{t - t_0} \int_{t_0}^t \|\mathbf{K}[\mathbf{x}(s); s]\| ds. \quad (7)$$

The fact that the right hand side of Eq. (7) is positive semi-definite implies that  $\Re[\Lambda_1]$  must be negative for there to be any chance of satisfying the rigorous condition.

Since the decomposition given by Eq. (4) is not unique an examination of  $\mathbf{K}$  in Eq. (7) is required. Notice that  $\|\mathbf{K}\| = \|\widetilde{\mathbf{D}}\mathbf{F} - \widetilde{\mathbf{Q}}\|$  where  $\widetilde{\mathbf{D}}\mathbf{F} \equiv \mathbf{P}^{-1} \mathbf{D} \mathbf{F} \mathbf{P}$  and  $\widetilde{\mathbf{Q}} \equiv \mathbf{P}^{-1} [\mathbf{A} + \mathbf{D}\mathbf{E}(\mathbf{0})] \mathbf{P}$ . Thus, the right hand side of Eq. (7) can be rewritten as

$$I = \lim_{t \rightarrow \infty} \frac{1}{t - t_0} \times \int_{t_0}^t \left[ \sum_{\alpha, \beta=1}^d (\widetilde{D}F_{\alpha\beta}[\mathbf{x}(s); s] - \widetilde{Q}_{\alpha\beta})^2 \right]^{1/2} ds,$$

where the ambiguity of the decomposition is confined to the matrix  $\widetilde{\mathbf{Q}}$ . The role of  $I$  in Eq. (7) leads us to conjecture that minimizing  $I$  produces the best chance for synchronization. We make this conjecture despite the fact that  $\Re[\Lambda_1]$  depends on this decomposition. Hence, we define the optimal value of  $\mathbf{Q} = \mathbf{A} + \mathbf{D}\mathbf{E}(\mathbf{0})$  as the one which minimizes  $I$ .

It is straightforward, by setting  $\partial I / \partial \widetilde{\mathbf{Q}} = \mathbf{0}$ , to show that the optimal value for  $\mathbf{Q}$  is given by

$$\mathbf{Q} = \lim_{t \rightarrow \infty} \frac{1}{t - t_0} \int_{t_0}^t \mathbf{D}\mathbf{F}[\mathbf{x}(s); s] ds \equiv \langle \mathbf{D}\mathbf{F} \rangle,$$

where  $\langle \bullet \rangle$  denotes a time average on the invariant measure  $\mathbf{x}(s)$ . This result implies that the optimal decomposition in Eq. (4) is

$$\mathbf{A} \equiv \langle \mathbf{D}\mathbf{F} \rangle - \mathbf{D}\mathbf{E}(\mathbf{0}), \quad (8)$$

$$\mathbf{B}(\mathbf{x}; t) \equiv \mathbf{D}\mathbf{F}(\mathbf{x}; t) - \langle \mathbf{D}\mathbf{F} \rangle, \quad (9)$$

and the condition for linear stability of the invariant trajectory in the synchronization manifold is

$$-\Re[\Lambda_1] > \langle \|\mathbf{P}^{-1}[\mathbf{B}(\mathbf{x}; t)] \mathbf{P}\| \rangle. \quad (10)$$

Equations (8)–(10) are the major results of this section. Together they represent definitions and a criterion which indicate when synchronous motion along a particular driving trajectory is guaranteed to be stable to small perturbations in directions transverse to the synchronization manifold. As indicated by our examples and Appendix C this criterion can be used to design couplings that are guaranteed to result in stable synchronization. Unfortunately, the criterion is only sufficient, not necessary *and* sufficient. Thus, one can expect, and our numerical experiments show, that it is possible for a coupling scheme to fail this criterion and still produce stable synchronization. This is due, in part, to the fact that the derivation of Eq. (10) involved inequalities of norms which will

tend to overestimate the necessary coupling strengths. The relationship between these results and control theory are discussed below in Appendix D.

As defined above, the decomposition in Eqs. (8) and (9) is optimal in the sense that it minimizes the right hand side of Eq. (10). We have conjectured that this gives one the best chance at satisfying the inequality. To support this conjecture we have the following circumstantial evidence. If we insert Eq. (9) into a Volterra expansion of Eq. (5), then, to second order, the criteria for linear stability is  $\Re[\Lambda_1] < 0$  (see the next section). For any other decomposition this simple approximate stability criteria is only correct to first order. If the driving trajectory is a fixed point, then  $\mathbf{B}(\mathbf{x};t) = \mathbf{0}$  and Eq. (10) reduces to  $\Re[\Lambda_1] < 0$ . This result is what one would expect from simple linear stability. However, it does not occur for other decompositions. To address the full optimality issue one must compare the size of  $\langle \|\mathbf{P}^{-1}\mathbf{B}\mathbf{P}\| \rangle$  to the size of the first eigenvalue of  $\mathbf{A}$ . We are unable to make this comparison due to the complicated dependence of the eigenvalues on the coupling strengths,  $\mathbf{DE}(\mathbf{0})$ . (The idea of using a time average to define  $\mathbf{A}$  is also suggested in Ref. 17.)

Because the stability criterion depends explicitly on the driving trajectory, the measure associated with the dynamics is of crucial importance. An early paper by Gupte and Amaritkar<sup>22</sup> used unstable periodic orbits as driving trajectories for synchronization. They (and others) found that, for fixed coupling strength, synchronization is stable for some driving trajectories and unstable for other driving trajectories.<sup>8,20</sup> In order to determine a coupling strength that results in a stable synchronization manifold (i.e., synchronous motion is stable on all possible driving trajectories), notice that the right hand side of Eq. (10) is a time average.

Recently, Hunt and Ott<sup>28</sup> examined time averages of functions for different measures of the dynamics of a chaotic system. They found that, for chaotic systems, time averages tend to take on their largest values for measures confined to the unstable periodic orbits with the shortest periods. (This effect was also observed in Ref. 14.) They also found that if an unstable periodic orbit with a somewhat higher period has the largest time average, then this value is usually only a small increase compared to orbits with lower periods. Therefore, if synchronization is stable for fixed points and periodic orbits (with short periods) located in the chaotic attractor, one may consider this as an indication that synchronized chaotic motion is also stable (an assumption also proposed in Ref. 8). This assumption is supported by the Hunt and Ott who claim that a nonperiodic orbit will yield the maximum time average on a set of measure zero in the parameter space associated with the parameters of  $\mathbf{F}$ . Finally, this paper presents a crude formula for determining how high in period one must look in order to insure that the largest time averages have been found. (The issue of obtaining time averages for dynamics on chaotic attractors by weighting time averages on the unstable periodic orbits has been addressed by Cvitanović.<sup>29</sup>)

In general the stability condition given by Eq. (10) requires that one integrate the norm of a matrix along the driving trajectory. As such these equations could be difficult to

use as an explicit test to determine whether a given coupling scheme will produce synchronization. (Despite this they are still far more efficient than the Lyapunov exponent approximations found in most other papers.) However, for simple systems, many of the important calculations can be performed analytically (see Section IV Appendix E, and Ref. 18 for examples). Therefore, the criterion of Eqs. (8)–(10), along with the results of Ref. 28, may well allow one to determine coupling schemes that insure linear stability of the entire synchronization manifold.

### III. THEORY PART II: APPROXIMATE RESULTS

Even with the rigorous results of the previous section one often desires a “quick and dirty” criterion to approximate whether a particular coupling scheme and/or coupling strength will produce linearly stable synchronous motion. The major result of this section is just such a criterion.

Begin by noting that an infinite series solution to Eq. (5) can be obtained by inserting this equation into itself to form a Volterra expansion<sup>30</sup>

$$\mathbf{z}(t) = \left[ \mathbf{U}(t, t_0) + \sum_{j=1}^{\infty} \mathbf{M}^{(j)}(t, t_0) \right] \mathbf{z}(t_0),$$

where

$$\begin{aligned} \mathbf{M}^{(j)}(t, t_0) &= \int_{t_0}^t ds_1 \int_{t_0}^{s_1} ds_2 \cdots \\ &\times \int_{t_0}^{s_{j-1}} ds_j \mathbf{U}(t, s_1) \mathbf{K}(s_1) \mathbf{U}(s_1, s_2) \mathbf{K}(s_2) \cdots \\ &\times \mathbf{K}(s_j) \mathbf{U}(s_j, t_0). \end{aligned}$$

Truncating this solution at  $j=1$  yields the following approximate solution to Eq. (5):

$$\mathbf{z}(t) \approx [\mathbf{U}(t, t_0) + \mathbf{M}^{(1)}(t, t_0)] \mathbf{z}(t_0). \quad (11)$$

(Provided the series is well behaved, it converges, etc., one can obtain better solutions than the one discussed below by retaining more terms in the series.) To this approximation if all elements of  $\mathbf{U} + \mathbf{M}^{(1)}$  decay in time, then  $\lim_{t \rightarrow \infty} \|\mathbf{z}(t)\| = 0$ , and synchronization is linearly stable.

It is useful to divide the discussion of  $\mathbf{M}^{(1)}$  into an analysis of diagonal and off-diagonal elements.

1. *Diagonal elements.* For these elements

$$\begin{aligned} [M^{(1)}]_{\alpha\alpha} &= \exp[\Lambda_{\alpha}(t - t_0)] \\ &\times \sum_{\mu, \nu=1}^d P_{\alpha\mu}^{-1} \left[ \left( \int_{t_0}^t DF_{\mu\nu}(s) ds \right) \right. \\ &\left. - \langle DF_{\mu\nu} \rangle (t - t_0) \right] P_{\nu\alpha} \end{aligned}$$

were the optimal decomposition of Eqs. (8) and (9) have been used. For this decomposition the term in large square brackets vanishes in the large  $t$  limit. For any other decomposition this term can be expected to grow at least linearly

with time. Depending on the strength of growth this term could offer significant competition to the anticipated exponential decay from  $\exp[\Lambda_\alpha(t-t_0)]$ .

2. *Off-diagonal elements.* For these elements

$$[M^{(1)}]_{\alpha\beta} = \exp(\Lambda_\alpha t - \Lambda_\beta t_0) \times \int_{t_0}^t \exp[(\Lambda_\beta - \Lambda_\alpha)s] K_{\alpha\beta}(s) ds.$$

For the dynamical systems we are examining the driving signal,  $\mathbf{x}$ , is bounded and the Jacobian is bounded (typically  $\mathbf{x}$  is confined to a compact attractor). Therefore,

$$[M^{(1)}]_{\alpha\beta} \leq \frac{K_{\alpha\beta}^{(\max)}}{\Lambda_\beta - \Lambda_\alpha} [\exp(\Lambda_\beta t) - \exp(\Lambda_\alpha t)],$$

where  $K_{\alpha\beta}^{(\max)}$  is the maximum value taken by  $K_{\alpha\beta}(s)$  on the driving trajectory and we have assumed the eigenvalues of  $\mathbf{A}$  are distinct.

This analysis of  $\mathbf{M}^{(1)}$  indicates that if  $\Re[\Lambda_1] < 0$ , then the off-diagonal elements of the matrix  $\mathbf{U} + \mathbf{M}^{(1)}$  die off exponentially for  $t > t_0$ , while the diagonal elements die off at a rate controlled by the convergence of the time average  $\langle \mathbf{DF} \rangle$ . Therefore, to second order we have the following simple condition for linear stability (to transverse perturbations) of a trajectory on the synchronization manifold

$$\Re[\Lambda_1] < 0. \tag{12}$$

Equation (12) is the major results of this section. It, and Eq. (8), represent a ‘‘quick and dirty’’ criterion to determine whether or not synchronization will occur for a particular coupling scheme.

Equation (12) is completely consistent with the rigorous results of the previous section. As expected the approximate criterion given by Eqs. (8) and (12) depends explicitly on the measure of the driving trajectory. An appealing aspect of Eq. (12) is that the analytic and computational burden associated with computing  $\mathbf{A}$  and its eigenvalues is relatively minor. Thus, one can quickly search over many types of coupling schemes.

Our numerical experiments show that Eq. (12) is actually a good approximation to the *minimum* coupling needed to achieve linearly stable synchronization. One possible explanation for the success of this approximation is a ‘‘folk theorem’’ from control theory discussed by Brogan.<sup>31</sup> ‘‘A commonly used stability analysis technique is the so-called frozen coefficient method, in which all time-varying coefficients are frozen and then the system stability is analyzed as if it were a constant coefficient system.’’<sup>31</sup> Brogan goes on to claim that ‘‘when used with caution, this approach will usually give the correct result.’’ As a final comment we note that Ref. 17 also examined  $\mathbf{A}$  to determine the linear stability of synchronization.

#### IV. NUMERICAL EXPERIMENTS

This section presents results from numerical experiments we have performed to test the conditions derived in Sections II and III. The results from the first example are mostly nu-

merical and focus on the approximate condition. By the last example almost all of the calculations are performed analytically and focus on both the rigorous and the approximate condition (see Appendix A for yet another example). When appropriate we will use  $\epsilon^{(c)}$  to denote critical coupling strengths where the driving trajectory on the synchronization manifold becomes linearly stable.

#### A. Rossler example

The Rossler system is the following set of three coupled ordinary differential equations (ODE’s)

$$\frac{dx}{dt} = -y - z,$$

$$\frac{dy}{dt} = x + ay,$$

$$\frac{dz}{dt} = b + z(x - c),$$

where  $a = 0.2$ ,  $b = 0.2$  and  $c = 9$ . For these parameter settings the dynamics of this system has a chaotic attractor, and two unstable fixed points located at  $\mathbf{x}_\pm = (-ay_\pm, y_\pm, -y_\pm)$  where

$$y_\pm = -\frac{c}{2a} \left[ 1 \pm \left( 1 - \frac{4ab}{c^2} \right)^{1/2} \right].$$

Only the fixed point at  $\mathbf{x}_-$  is near the attractor.

To simplify matters we use diagonal coupling,  $\mathbf{E}(\mathbf{x} - \mathbf{y}) = \text{diag}(\epsilon_1, \epsilon_2, \epsilon_3) \cdot (\mathbf{x} - \mathbf{y})$ . For this type of coupling it is easy to show that Eq. (8) leads to

$$\mathbf{A} = \begin{bmatrix} -\epsilon_1 & -1 & -1 \\ 1 & a - \epsilon_2 & 0 \\ \langle z \rangle & 0 & \langle x \rangle - c - \epsilon_3 \end{bmatrix}.$$

Our numerical experiments examine four different measures of the driving dynamics. One is the natural or Sinai–Bowen–Ruelle (SBR) measure on the chaotic attractor. This arises from following an arbitrary trajectory on the chaotic attractor. The others are Dirac measures associated with the  $\mathbf{x}_-$  fixed point, and unstable period 1 and period 2 orbits. The trajectories associated with the fixed point and the periodic orbits are shown in Fig. 1.

Because the characteristic equation for  $\mathbf{A}$  is a cubic that can not be easily factored for arbitrary values of the  $\epsilon$ ’s, most of the results were obtained numerically. (We have calculated these eigenvalues using a symbolic manipulator to perform the necessary algebra. The expressions are not particularly enlightening, and will not be presented.)

#### 1. Fixed point measure

On this measure  $\mathbf{B}(\mathbf{x}; t) = \mathbf{0}$ , so the rigorous and approximated criterion are both  $\Re[\Lambda_1] < 0$  (a familiar result from stability analysis of fixed points found in textbooks). Figure 2 shows the real parts of the eigenvalues of  $\mathbf{A}$  as functions of  $\epsilon \equiv \epsilon_1$  when the driving trajectory is  $\mathbf{x}_-$  and we only use the first component of  $\mathbf{x}_-$  as the driving signal ( $\epsilon_2 = \epsilon_3 = 0$ ).

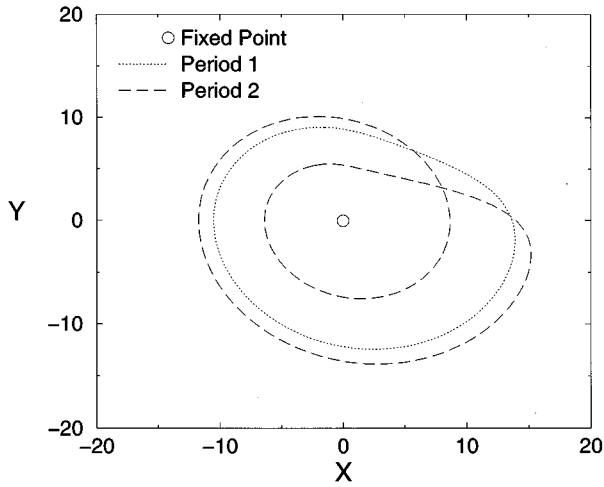


FIG. 1. Fixed point, period 1 and period 2 orbits of the Rossler systems.

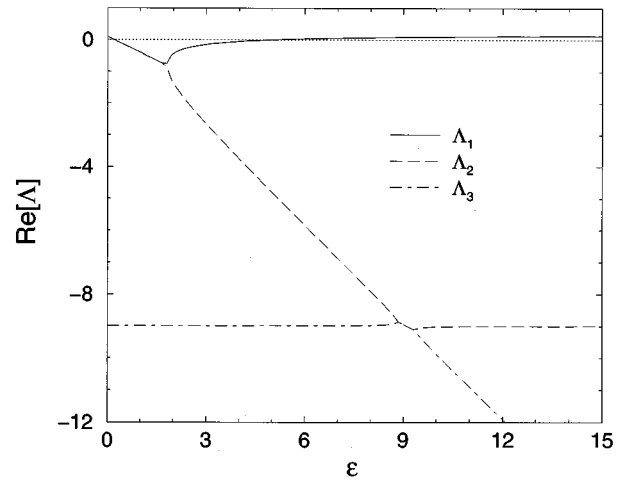


FIG. 2. The real parts of the eigenvalues of  $\mathbf{A}$  as functions of  $\epsilon$  for  $x$ -driving.  $\mathbf{A}$  comes from the Rossler system and the driving trajectory is the fixed point  $\mathbf{x}_-$ . The dashed line at  $\Lambda=0$  is inserted as a visual aid.

This type of driving is typically called  $x$ -driving. (A dotted line at  $\Lambda=0$  is inserted as a visual aid.) The figure indicates that, initially,  $\Lambda_1$  and  $\Lambda_2$  are complex conjugate pairs with positive real parts. However, as  $\epsilon$  increases the real parts become negative at  $\epsilon^{(c)}=0.19750\dots$ . As  $\epsilon$  continues to increase  $\Lambda_1$  and  $\Lambda_2$  become real at  $\epsilon \approx 1.8$ , with  $\Lambda_1$  increasing and  $\Lambda_2$  decreasing.  $\Lambda_1$  eventually becomes positive at  $\epsilon=4.9975\dots$ . The figure also indicates that  $\Lambda_2$  and  $\Lambda_3$  merge into complex conjugate pairs but soon split back into pure reals at  $\epsilon \approx 9$ . If the second component of  $\mathbf{x}_-$  is used as the driving signal ( $y$ -driving), then a similar figure is produced, however  $\Lambda_1$  remains negative for large  $\epsilon$ .

The interesting feature of Fig. 2 is the prediction of synchronous behavior for  $x$ -driving when  $\epsilon$  is in the range between about 0.2 and about 5. Although no numerical experiment can prove the correct values of  $\epsilon^{(c)}$ , our experiments indicates that when  $x$ -driving is used a bifurcation from un-

stable (stable) synchronization to a stable (unstable) synchronization appears to occur at  $\epsilon^{(c)}=0.19750\dots$  (4.9975\dots).

The results of all of our numerical experiments on the Rossler system appear in Table I. The table indicates that for both  $x$ - and  $y$ -driving synchronization to  $\mathbf{x}_-$  begins at  $\epsilon^{(c)} \approx 0.2$ . For  $x$ -driving synchronization ends at  $\epsilon^{(c)} \approx 4.9$ , while for  $y$ -driving it persists for arbitrarily large values of  $\epsilon$ . When  $z$ -driving is used  $\Lambda_1$  and  $\Lambda_2$  are complex conjugate pairs with positive real parts throughout the entire range of  $\epsilon$ . Thus, the rigorous and approximate conditions predict that synchronization will not occur at  $\mathbf{x}_-$  for this type of driving. The numerical experiments appear to verify this result. (We remark that the rigorous condition predicts, and we were able to verify, a range of values for  $\epsilon$  which will result in synchronization about  $\mathbf{x}_+$  for  $z$ -driving.)

TABLE I. Results of numerical tests on the Rossler system. In this table F implies that this type of driving fails the test, while None implies that synchronization did not occur.

Measure type	Drive type	Rossler system Approximate test		Numerical test	
		$\epsilon_{\min}^{(c)}$	$\epsilon_{\max}^{(c)}$	$\epsilon_{\min}^{(c)}$	$\epsilon_{\max}^{(c)}$
Fixed point	$x$	0.1975	4.998	0.1975	4.998
	$y$	0.1976	$\infty$	0.1976	$\infty$
	$z$	9.0	225	9.0	225
Period 1	$x$	0.04	4.8	0.54	3.7
	$y$	0.04	$\infty$	0.36	$\infty$
	$z$	F	F	None	
Period 2	$x$	0.07	4.9	0.32	4.3
	$y$	0.07	$\infty$	0.29	$\infty$
	$z$	F	F	None	
SBR	$x$	0.11	4.9	0.20	4.5
	$y$	0.11	$\infty$	0.18	$\infty$
	$z$	F	F	None	

TABLE II. Numerical estimates for averages along driving trajectories. For the Rossler system  $\langle x \rangle = -a \langle y \rangle$  and  $\langle z \rangle = -\langle y \rangle$ .

Measure Type	Rossler system			Lorenz system		
	$\langle x \rangle$	$\langle y \rangle$	$\langle z \rangle$	$\langle x \rangle$	$\langle y \rangle$	$\langle z \rangle$
Period 1	0.2770	-1.385	1.385	0	0	54.81
Period 2	0.2246	-1.123	1.123	0	0	54.94
SBR	0.1649	-0.8245	0.8245	0	0	54.82

**2. Periodic orbit measures**

On these measures (as well as the SBR measure)  $\mathbf{B}(\mathbf{x}; t) \neq \mathbf{0}$ , so the rigorous and approximate criterion are not the same. We will only consider the approximate condition and save a discussion of the rigorous condition for later examples.

The matrix  $\mathbf{A}$  is a function of time averages over the driving trajectory. Table II shows numerically determined values for  $\langle x \rangle$ ,  $\langle y \rangle$ , and  $\langle z \rangle$  on each of our measures.

Numerical experiments using the measure associated with periodic orbits indicate that the eigenvalues of  $\mathbf{A}$  undergo the same type of splittings and mergings found for the fixed point case. More importantly for the period 1 (2) orbit  $\Re[\Lambda_1]$  becomes negative at  $\epsilon \approx 0.04$  (0.07) for both  $x$ - and  $y$ -driving. In addition, for  $x$ -driving and the period 1 (2) orbit,  $\Re[\Lambda_1]$  becomes positive at  $\epsilon \approx 4.84$  (4.87). When  $y$ -driving is used  $\Lambda_1$  remains negative for large  $\epsilon$ . The approximate criteria predicts a change in stability each time  $\Re[\Lambda_1]$  changes sign.

The results of numerical experiments to test these predictions are shown in Fig. 3. The figure indicates that if  $x$ -driving is used and  $\epsilon = 0.53$ , then the response system remains a finite distance from the period 1 orbit. However, if  $\epsilon = 0.54$ , then the driven dynamics exponentially converges onto the period 1 orbit. The figure also shows that if  $\epsilon = 3.8$ , then the response system appears to diverge while it exponentially converges to the period 1 orbit for  $\epsilon = 3.7$ .

As shown in Table I, numerical tests of these predictions indicate that the lower (higher) critical coupling strength is higher (lower) than that predicted by the approximate criterion. Thus, the range of coupling strengths for which synchronization occurs is slightly smaller than that predicted by the approximate criterion. This is to be expected since the rigorous criterion implies that it is not enough that  $\Re[\Lambda_1]$  be negative, it must be sufficiently negative to overcome the fluctuations represented by  $\langle \|\mathbf{P}^{-1} \mathbf{B} \mathbf{P}\| \rangle$ . However, given the ‘‘quick and dirty’’ nature of the approximate criterion we believe that it yields reasonable predictions for coupling strengths that produce synchronization.

**3. SBR measure**

The results of tests conducted on the SBR measure are much more complicated than those obtained on the simple measures examined above. Sample plots of  $\|\mathbf{y} - \mathbf{x}\|$  for various values of  $\epsilon$  and types of driving are shown in Fig. 4. These figures indicate the bursting phenomena observed by previous researchers when discussing synchronization. The

degree to which the response system is ‘‘synchronized’’ to the drive system clearly depends on the degree to which one is willing to tolerate bursts.

For example, when  $y$ -driving is used Fig. 4(b) indicates that  $\|\mathbf{y} - \mathbf{x}\| \sim 10^{-4}$  can occur for as long as 1000 times around the attractor before climbing to  $\|\mathbf{y} - \mathbf{x}\| \sim 1$ . (For

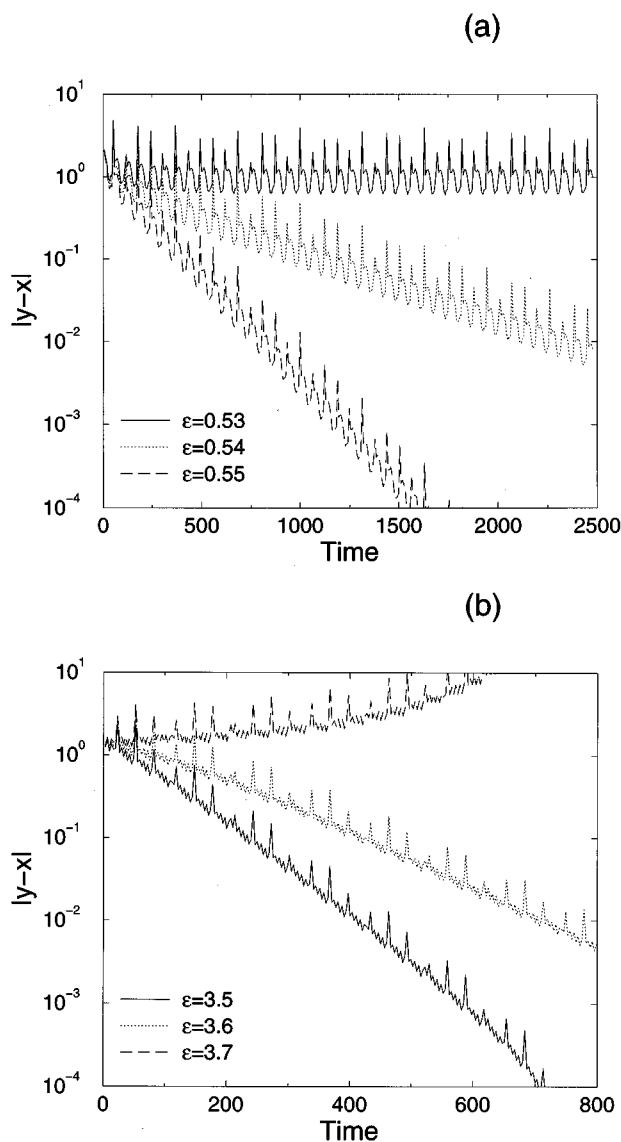


FIG. 3. Results of numerical test for critical coupling strengths. The Rossler system synchronized to the period 1 orbit. The period of the orbit is approximately six units of time and  $x$ -driving is used. (a) Output is every 106/96th of the period. (b) Output is every 53/96th of the period.

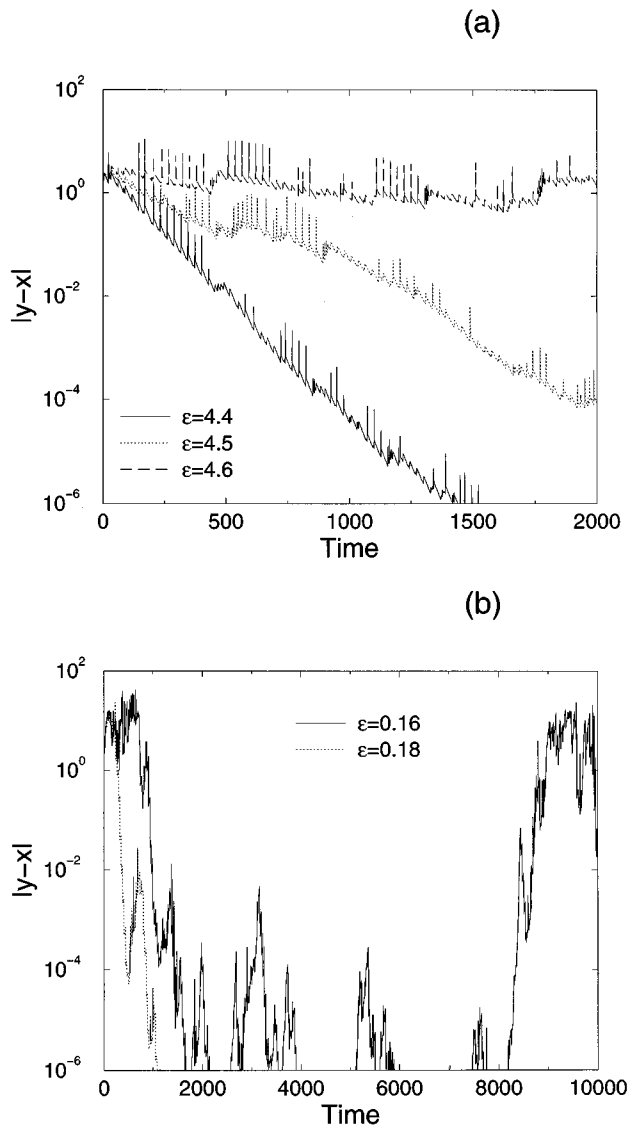


FIG. 4. Results of numerical test for critical coupling strengths. The Rossler system synchronized to a chaotic trajectory. (a)  $x$ -driving with output every one unit of time. (b)  $y$ -driving with output every two units of time.

$\epsilon=0.15$  we have observed  $\|y-x\| < 10^{-4}$  for as many as 4000 times around the attractor.) These examples confirm that one must be cautious about discussing the condition for linear stability of synchronization when the SBR measure is used. The values shown in Table I were selected because  $\|y-x\|$  steadily decayed to a small value and did not significantly increase for the next 50 000 time steps. In addition we required that  $\|y-x\|$  exhibit the same behavior for values of  $\epsilon$  close to  $\epsilon^{(c)}$  and on the stable side of the threshold.

However, because SBR trajectories are dense they will eventually come arbitrarily close to any unstable trajectory. The values of  $\epsilon^{(c)}$  listed in Table I for the SBR measure are outside the range listed for the period 1 and period 2 orbits. Therefore, if the SBR orbit comes sufficiently close to either of these orbits and/or stays close for a sufficiently long time, then a burst could happen.<sup>20</sup> The results implied by Table I indicate that for our numerical experiments the SBR trajec-

tory did not come sufficiently close to either the period 1 or period 2 orbits.

**B. Lorenz example**

The Lorenz system is the following set of three coupled ODE's:

$$\begin{aligned} \frac{dx}{dt} &= \sigma(y-x), \\ \frac{dy}{dt} &= rx-y-xz, \\ \frac{dz}{dt} &= xy-bz, \end{aligned}$$

where  $\sigma=10$ ,  $b=8/3$ , and  $r=60$ . For these parameter values the dynamics of the system has a chaotic attractor and three unstable fixed points, one of which is at the origin.

This example is particularly instructive because if the coupling is given by

$$DE(0) = \begin{bmatrix} \epsilon_1 & \epsilon_4 & 0 \\ \epsilon_3 & \epsilon_2 & 0 \\ 0 & 0 & \epsilon_z \end{bmatrix},$$

then many of the calculations can be performed analytically. Furthermore, this type of coupling allows the  $x$  or  $y$  variable to drive both the  $x$  and  $y$  equations. Ott and Ding<sup>23</sup> have shown that this type of coupling is useful when not all variables are measurable. Their work, and the result presented below, indicates that this type of driving may produce or guarantee synchronization when purely diagonal coupling does not.

For this dynamical system it is easy to show that Eq. (8) leads to

$$A = \begin{bmatrix} -\sigma - \epsilon_1 & \sigma - \epsilon_4 & 0 \\ r - \langle z \rangle - \epsilon_3 & -1 - \epsilon_2 & -\langle x \rangle \\ \langle y \rangle & \langle x \rangle & -b - \epsilon_z \end{bmatrix}.$$

We examine the SBR measure and Dirac measures associated with the fixed point at the origin, a period 1, and a period 2 orbit. The trajectories associated with these measures are shown in Fig. 5. Table II shows numerically calculated values for  $\langle x \rangle$ ,  $\langle y \rangle$ , and  $\langle z \rangle$ , on each of these trajectories. The eigenvalues of  $A$  are

$$\begin{aligned} \Lambda_z &= -b - \epsilon_z, \\ \Lambda_{\pm} &= \frac{-(\sigma + 1 + \epsilon_1 + \epsilon_2)}{2} \pm \frac{1}{2} \left( [(\sigma + \epsilon_1) - (1 + \epsilon_2)]^2 + 4(\sigma - \epsilon_4)(r - \langle z \rangle - \epsilon_3) \right)^{1/2}, \end{aligned} \tag{13}$$

and, in practice,  $\Lambda_1$  could be either  $\Lambda_+$  or  $\Lambda_-$ .

**1. Fixed point measures**

On these measures  $B(x;t) = 0$ , and the rigorous and approximate criterion are both  $\Re[\Lambda_1] < 0$ . Because  $\Lambda_z = -b - \epsilon_z < 0$  for all positive values of  $\epsilon_z$ , we focus our

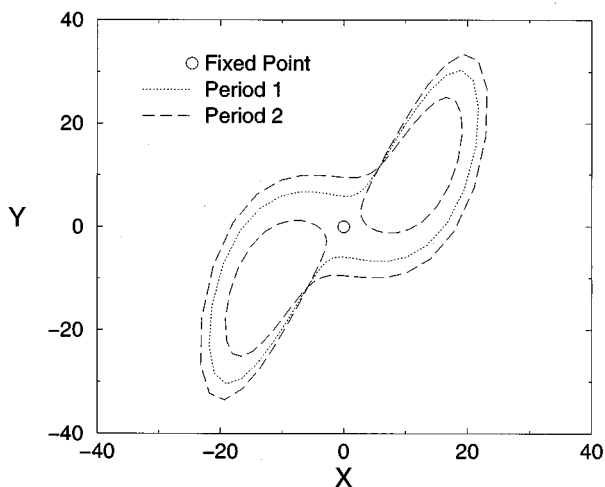


FIG. 5. Fixed point, period 1 and period 2 orbits of the Lorenz system.

attention on  $\Lambda_{\pm}$ . Analysis of Eq. (13) indicates that if diagonal  $x$ -driving is used ( $\epsilon_2 = \epsilon_3 = \epsilon_4 = 0$ ), then the critical coupling strength associated with  $\Re[\Lambda_1] = 0$  is  $\epsilon_1^{(c)} = \sigma(r-1) = 590$ . If diagonal  $y$ -driving is used ( $\epsilon_1 = \epsilon_3 = \epsilon_4 = 0$ ), then the critical coupling strength is  $\epsilon_2^{(c)} = r-1 = 59$ . Finally, it is easy to show that if diagonal  $z$ -driving is used, then  $\epsilon_1 = \epsilon_2 = \epsilon_3 = \epsilon_4 = 0$  and  $\Re[\Lambda_1] > 0$ . Therefore, for  $z$ -driving the rigorous criterion can not be satisfied. The results of all of our numerical experiments on the Lorenz system appear in Table III.

**2. Periodic orbit measures**

On these measures (as well as the SBR measure)  $\mathbf{B}(\mathbf{x}; t) \neq \mathbf{0}$ . An analysis of the approximate condition of Eq. (12), in conjunction with Eq. (13), indicates that the approximation to the critical coupling strength is  $\epsilon_1 = \sigma[r - \langle z \rangle - 1] \approx 42$  for diagonal  $x$ -driving, and  $\epsilon_2 = r - \langle z \rangle - 1 \approx 4.2$  for diagonal  $y$ -driving. Numerical ex-

periments on the period 1 orbit are shown in Fig. 6. They indicate that  $\epsilon_1^{(c)} \approx 17$  for  $x$ -driving and  $\epsilon_2^{(c)} \approx 4.2$  for  $y$ -driving. Although the error in our approximation for  $x$ -driving may appear large, comparing it to the value  $\epsilon^{(c)} = 590$  needed for the fixed point at the origin indicates that it may not be very large.

**3. SBR measure**

Results of the tests conducted on the SBR measure are much more complicated than those obtained on the simple measures examined above. Figure 7 exhibits the bursting behavior observed when the trajectory of the response system approaches a region of phase space that is unstable to perturbations perpendicular to the synchronization manifold. Because SBR trajectories are dense they will eventually encounter any such region. Thus, although Fig. 7(a) appears to indicate that the system will synchronize when  $\epsilon_1 > 18$  for  $x$ -driving, we know that the fixed point at the origin is unstable for this value of  $\epsilon_1$ . Therefore, if the trajectory comes sufficiently close to  $\mathbf{x} = \mathbf{0}$ , then a burst will occur.

**C. Ott–Sommerer example**

The third dynamical system we examine is the Ott–Sommerer<sup>21</sup> set of four nonautonomous ODE’s:

$$\begin{aligned} \frac{dx}{dt} &= v_x, \\ \frac{dv_x}{dt} &= -\nu v_x + 4x(1-x^2) + y^2 + f_0 \sin(\omega t), \\ \frac{dy}{dt} &= 2v_y, \\ \frac{dv_y}{dt} &= -\nu v_y - 2y(x-p) - 4ky^3, \end{aligned} \tag{14}$$

TABLE III. Results of numerical tests on the Lorenz system. In this table F implies that this type of driving fails the test, while None implies that synchronization did not occur.

Measure type	Drive type	Lorenz system			
		Approximate test		Numerical test	
		$\epsilon_{\min}^{(c)}$	$\epsilon_{\max}^{(c)}$	$\epsilon_{\min}^{(c)}$	$\epsilon_{\max}^{(c)}$
Fixed point	$x$	590	$\infty$	590	$\infty$
	$y$	59	$\infty$	59	$\infty$
	$z$	F	F	None	
Period 1	$x$	42	$\infty$	17	$\infty$
	$y$	4.2	$\infty$	4.1	$\infty$
	$z$	F	F	None	
Period 2	$x$	42	$\infty$	18	$\infty$
	$y$	4.2	$\infty$	4.0	$\infty$
	$z$	F	F	None	
SBR	$x$	42	$\infty$	19	$\infty$
	$y$	4.2	$\infty$	4.0	$\infty$
	$z$	F	F	None	

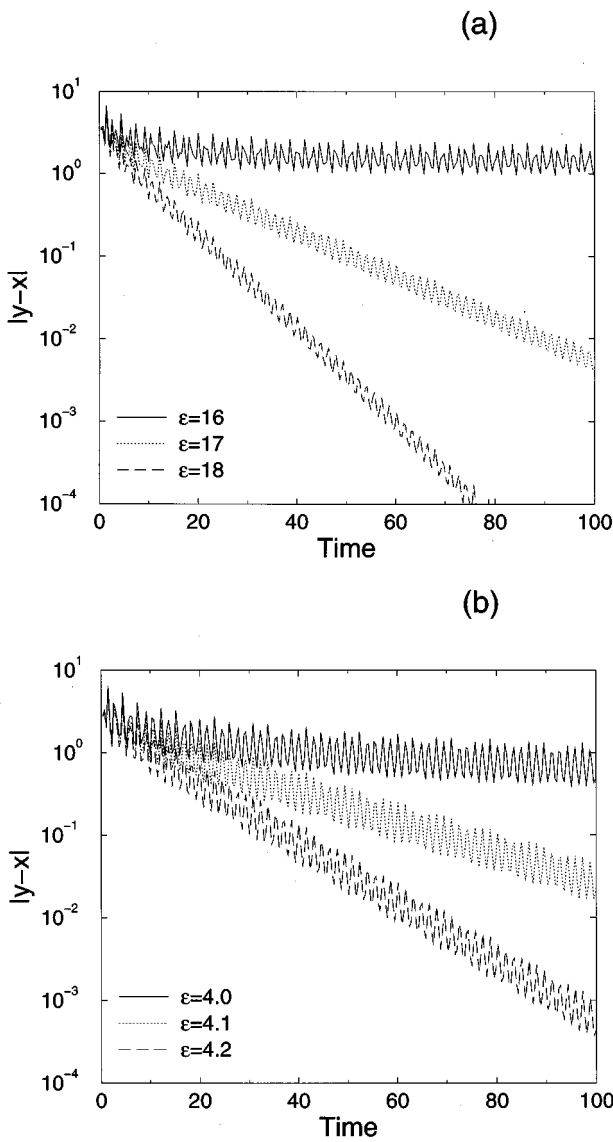


FIG. 6. Results of numerical test for critical coupling strengths. The Lorenz system synchronized to a period 1 orbit. The period of the orbit is approximately one unit of time and output is every 19/50th of the period. (a) x-driving. (b) y-driving.

where  $\nu=0.05$ ,  $f_0=2.3$ ,  $\omega=3.5$ ,  $k=0.0075$  and  $p=-1.5$ . This example is interesting for at least two reasons:

- (1) From the point of view of synchronization, it possesses a rich structure of invariant manifolds.
- (2) For the case we will examine, *all* of the important calculations can be performed analytically.

Originally, Ott and Sommerer examined the two dimensional invariant manifold defined by  $y=v_y=0$  in the context of riddled basins. Their results indicate that motion on the manifold is chaotic, however, for our parameter values, the manifold is unstable. Thus, typical motion for this dynamical system is in  $\mathbb{R}^4$ , where there is one chaotic attractor and no other attracting sets.

As usual, denote the drive and response systems by

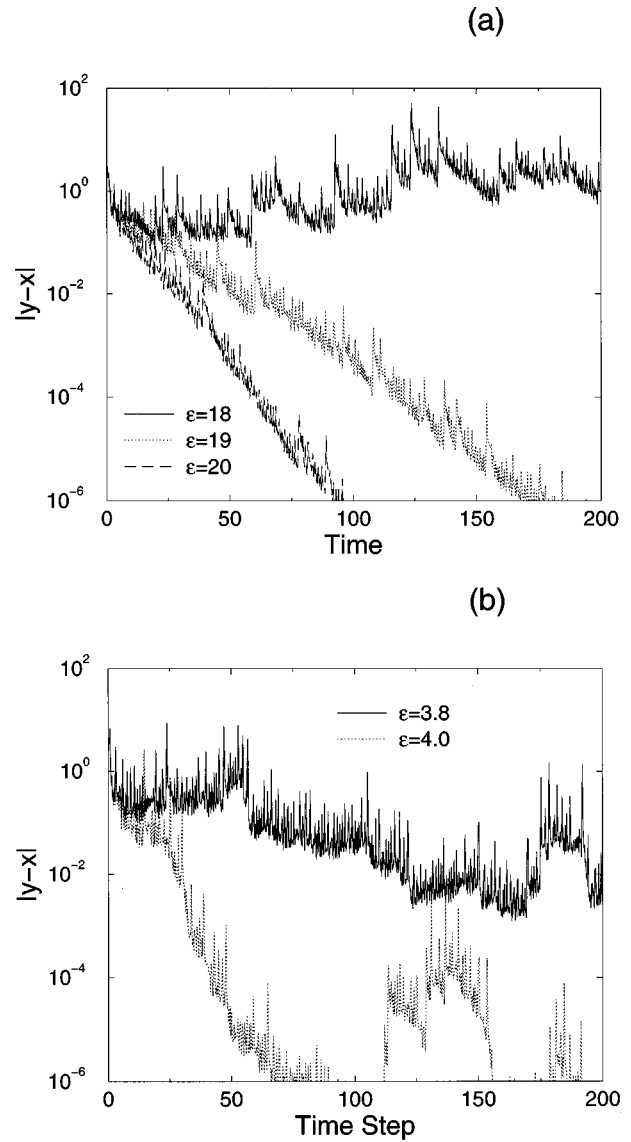


FIG. 7. Results of numerical test for critical coupling strengths. The Lorenz system synchronized to a chaotic trajectory. The output is every 1/4 units of time. (a) x-driving. (b) y-driving.

$$\frac{dx}{dt} = \mathbf{F}(\mathbf{x};t)$$

and

$$\frac{dy}{dt} = \mathbf{F}(\mathbf{y};t) + \mathbf{E}(\mathbf{x}-\mathbf{y}),$$

respectively.

In principle the driving trajectory  $\mathbf{x}=[x, v_x, y, v_y] \in \mathbb{R}^4$ ; however, we will consider driving trajectories restricted to the invariant manifold of the driving system. Under these circumstances,  $\mathbf{x}=[x, v_x, 0, 0]$  and  $\mathbf{DF}$  assumes a block diagonal form. If we use a block diagonal coupling matrix,  $\mathbf{DE}$ , then the linearized equation of motion for  $\mathbf{w}=\mathbf{y}-\mathbf{x}$  decomposes into motion parallel to, and perpendicular to, the invariant manifold of the system,

$$\frac{d\mathbf{w}^{(\perp)}}{dt} = [\mathbf{DF}^{(\perp)}(\mathbf{x}) - \mathbf{DE}^{(\perp)}(\mathbf{0})]\mathbf{w}^{(\perp)}, \quad (15)$$

where

$$\mathbf{DF}^{(\perp)}(\mathbf{x}) = \begin{bmatrix} 0 & 1 \\ g^{(\perp)}(x) & -\nu \end{bmatrix}$$

and

$$\mathbf{DE}^{(\perp)}(\mathbf{0}) = \begin{bmatrix} \epsilon_1^{(\perp)} & \epsilon_4^{(\perp)} \\ \epsilon_3^{(\perp)} & \epsilon_2^{(\perp)} \end{bmatrix},$$

and  $g^{(\perp)}(x) \equiv -2(x-p)$ .

An equation similar to Eq. (15) involving  $\mathbf{w}^{(\parallel)}$ ,  $\mathbf{DF}^{(\parallel)}$ ,  $\mathbf{DE}^{(\parallel)}$ , and  $g^{(\parallel)}(x) \equiv 4(1-3x^2)$  exists for motion parallel to the manifold. This decomposition implies, and our numerical experiments verify, that coupling strengths exist for which the response trajectory collapses onto the invariant manifold of the response system but the response system is still not synchronized to the driving system. When this occurs, the response system is linearly stable to perturbations perpendicular to this manifold but not to perturbations parallel to this manifold.

For the remaining discussion we drop the superscripts  $\perp$  and  $\parallel$ , and leave it to the reader to remember that each calculation must be performed in *both* the perpendicular and parallel subspaces. Using Eq. (15) it is easy to show that

$$\mathbf{A} = \begin{bmatrix} -\epsilon_1 & 1 - \epsilon_4 \\ \langle g \rangle - \epsilon_3 & -(\nu + \epsilon_2) \end{bmatrix}$$

and

$$\mathbf{B}(\mathbf{x}; t) = \begin{bmatrix} 0 & 0 \\ g(x) - \langle g \rangle & 0 \end{bmatrix}.$$

The eigenvalues of  $\mathbf{A}$  are

$$\Lambda_{\pm} = \frac{-(\nu + \epsilon_1 + \epsilon_2)}{2} \pm \frac{1}{2} [(\nu + \epsilon_2 - \epsilon_1)^2 + 4(1 - \epsilon_4)(\langle g \rangle - \epsilon_3)]^{1/2}, \quad (16)$$

and the eigenvectors are  $N_{\pm} \hat{\mathbf{e}}_{\pm} = [(1 - \epsilon_4), \epsilon_1 + \Lambda_{\pm}]$ , where  $N_{\pm}$  are the following normalizations  $N_{\pm} = [(1 - \epsilon_4)^2 + |\epsilon_1 + \Lambda_{\pm}|^2]^{1/2}$ . The eigenvalues of  $\mathbf{A}$  can be real or complex, depending on the values of the  $\epsilon$ 's. Using the eigenvectors,  $\hat{\mathbf{e}}_{\pm}$ , and the equation for  $\mathbf{B}$ , one can obtain the following simple expression (in each subspace)

$$\begin{aligned} \langle \|\mathbf{P}^{-1}[\mathbf{B}(\mathbf{x}; t)]\mathbf{P}\| \rangle &= \langle |g - \langle g \rangle| \rangle \\ &\times \left[ \frac{(1 - \epsilon_4)^2}{|\Lambda_- - \Lambda_+|^2} \right]^{1/2} \left[ \frac{N_+^2 + N_-^2}{N_+ N_-} \right]. \end{aligned}$$

Note that this equation for  $\langle \|\mathbf{P}^{-1}[\mathbf{B}(\mathbf{x}; t)]\mathbf{P}\| \rangle$  diverges at the transition between real and complex  $\Lambda_{\pm}$ 's. From Eq. (16) it is easy to see that  $\Re[\Lambda_1]$  increases as the term inside the square root increases from zero. Also, if  $\Lambda_{\pm}$  are complex, then  $-\Re[\Lambda_1]$  can be made arbitrarily large by increasing  $\epsilon_1$  and/or  $\epsilon_2$ . These observations suggest that the best hope for

satisfying the rigorous condition of Eq. (10) is to choose  $\epsilon$ 's so that  $\Lambda_{\pm}$  are complex with imaginary parts that are not too small.

It is easy to show that if  $\Lambda_{\pm}$  are complex, then  $N_+ = N_-$  and the rigorous condition for linear stability of synchronization is

$$\nu + \epsilon_1 + \epsilon_2 > 4 \langle |g - \langle g \rangle| \rangle C, \quad (17)$$

where

$$C = \left[ \frac{-(1 - \epsilon_4)^2}{(\nu + \epsilon_2 - \epsilon_1)^2 + 4(1 - \epsilon_4)(\langle g \rangle - \epsilon_3)} \right]^{1/2}. \quad (18)$$

(A similar, although more complicated, expression for  $C$  can be obtained when  $\Lambda_{\pm}$  are real.)

The major theoretical results of this example are Eqs. (16)–(18) and the conjecture that the  $\epsilon$ 's should be chosen so that  $\Lambda_{\pm}$  are complex. Together they represent an analytic solution to the rigorous criteria for synchronization.

Equation (17) is interesting because the right hand side depends on both the coupling strengths and the driving trajectory, while the left hand side only depends on the coupling strengths. A useful trick is to set  $C = \text{const.} > 0$ . Under these circumstances the right hand side of Eq. (17) is constant for a given driving trajectory and one can increase the value of  $\epsilon_1$  and  $\epsilon_2$  (maintaining constant  $C$ ) until the rigorous condition is satisfied. (As discussed in Appendix C this approach to designing couplings that satisfy the rigorous criterion is quite general.)

Because Eqs. (14) are nonautonomous, they do not have fixed points. However, periodic orbits and the SBR measure still exist. We examine the SBR and the Dirac measures associated with a period 1 and a period 2 orbit (see Fig. 8). Numerically calculated values for  $\langle g \rangle$  and  $\langle |g - \langle g \rangle| \rangle$  on each of these measures are shown in Table IV.

We now present examples where the rigorous criterion is tested for various types of driving. (Our theoretical and numerical results are summarized in Table V.) Our analysis is simple and is designed to show whether or not the rigorous criteria can be satisfied. Thus the numbers shown in Table V are quite large. As we show in Appendix C, the region of parameter space that results in couplings which satisfy the rigorous criteria typically has positive volume. Thus, with some additional effort we could have found lower values for the coupling strengths than those listed in Table V.

### 1. Diagonal driving

This type of driving uses all components of  $\mathbf{x}$  as the driving signal,  $\epsilon_3 = \epsilon_4 = 0$ , and  $\epsilon_1 = \epsilon_2 \equiv \epsilon$ . For this case the usable parameter space is the real line  $\mathbb{R}$  and rigorous results have been previously obtained.<sup>1,7</sup> For this type of driving Eq. (16) and Table IV indicate that  $\Lambda_{\pm}$  are always complex on each of our measures. In addition, Eq. (18) shows that  $C$  is independent of  $\epsilon$ , and its value is fixed by the driving trajectory. Inserting these results into Eq. (17) leads to the following expression for the rigorous condition for synchronization

$$\epsilon > -\frac{\nu}{2} + 2 \langle |g - \langle g \rangle| \rangle \left[ \frac{-1}{\nu^2 + 4 \langle g \rangle} \right]^{1/2}. \quad (19)$$

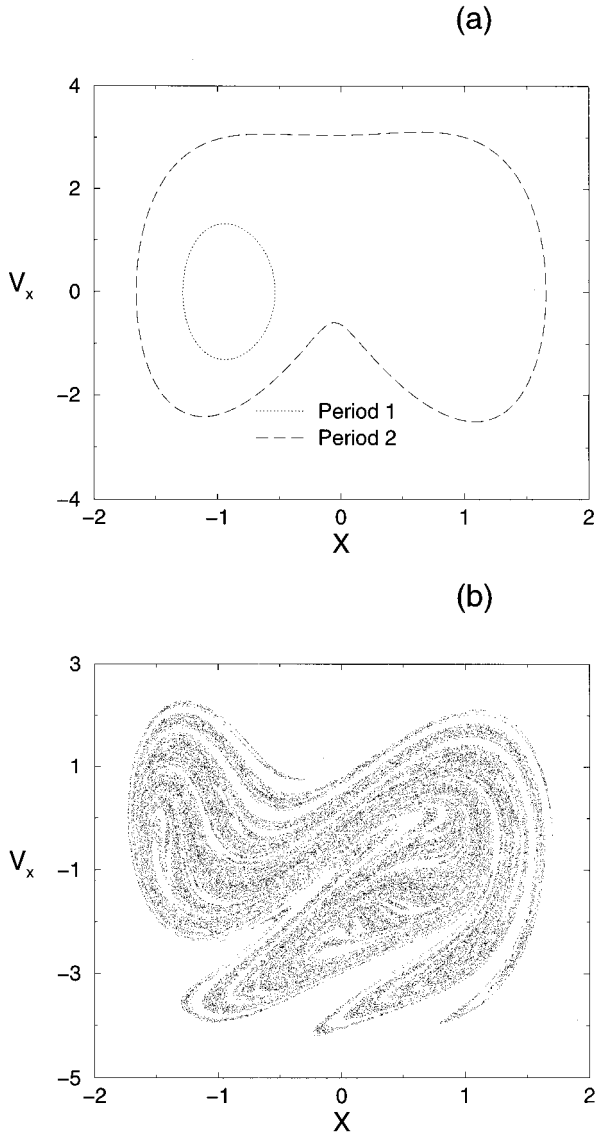


FIG. 8. Measures of the Ott-Sommerer model. (a) Period 1 and period 2 orbits. (b) The SBR orbit on the surface of section given by  $\omega t = 0 \pmod{2\pi}$ .

Since, for the considered examples, this condition can *always* be satisfied linearly stable synchronization can always be achieved with diagonal driving.

**2. Driving via position**

This type of driving uses only the position variables,  $x$  and  $y$ . The simplest example is when  $\epsilon_2 = \epsilon_3 = \epsilon_4 = 0$  and the parameter space is again  $\mathbb{R}$ . In order to demonstrate that the

rigorous criterion can not be satisfied for this type of driving we define new parameters  $u \equiv \epsilon_1 + \nu$  and  $w \equiv 1/C$ . In terms of the new parameters Eqs. (17) and (18) are

$$uw > 4|\langle g - \langle g \rangle |,$$

$$-4\langle g \rangle = (u - 2\nu)^2 + w^2.$$

On the measures we are considering  $\langle g \rangle < 0$ , so these equations define a hyperbola and a circle, respectively. The circle constrains the values of the new parameters to a one dimensional curve. Thus, the dimension of the usable parameter space is the same for new and old parameters. ( $C$  is imaginary for values of  $\epsilon_1 \in \mathbb{R}$  corresponding to points off the circle.)

Synchronization to the driving trajectory will be linearly stable if any portion of the circle extends above the hyperbola. It is straightforward to show that, on the measures we are examining, the hyperbola has  $w > [-4\langle g \rangle]^{1/2}$  when  $u - 2\nu = [-4\langle g \rangle]^{1/2}$ . Thus the hyperbola and the circle never intersect and the rigorous condition for synchronization can not be satisfied. (This result does not mean that this type of driving *will not* produce synchronization. It only means that our analysis can not determine a value of  $\epsilon_1$  that *guarantees* synchronization.)

Another variation of this type of driving uses the position variables to drive both the position *and* the velocity equation (see Ref. 23). For this type of driving  $\epsilon_2 = \epsilon_4 = 0$  and the parameter space, associated with  $\epsilon_1$  and  $\epsilon_3$ , is  $\mathbb{R}^2$ . Also, Eq. (16) and Table IV indicate that  $\Lambda_{\pm}$  are not complex for all values of  $\epsilon_1$  and  $\epsilon_3$ . However, if Eq. (18) is satisfied, then  $\Lambda_{\pm}$  are complex. Rewriting Eqs. (17) and Eq. (18) leads to the following expression for the rigorous condition for linearly stable synchronization:

$$\epsilon_1 > -\nu + 4C|\langle g - \langle g \rangle |, \tag{20}$$

$$\epsilon_3 = \frac{1}{4}(\nu - \epsilon_1)^2 + \left[ \langle g \rangle + \frac{1}{4C^2} \right], \tag{21}$$

where  $C > 0$  is arbitrary.

These equations define a line and a parabola, respectively. The parabola exist for all possible values of  $\epsilon_1$ , and all driving trajectories, and its minimum value is determined by the arbitrary constant  $C$ . The line also exists for all driving trajectories. (Of course one should choose  $C$  so that this line is in the positive  $\epsilon_1$  half plane.) These curves are guaranteed to intersect, and synchronization is guaranteed to be linearly stable for any point on the parabola whose  $\epsilon_1$  value is larger than the one associated with this intersection. We remark that  $C = 1/4|\langle g - \langle g \rangle |$  is a choice which greatly sim-

TABLE IV. The values of  $\langle g \rangle$  and  $|\langle g - \langle g \rangle |$  calculated on the measures shown in Fig. 8.

Measure Type	Ott-Sommerer System			
	$\langle g^{(\perp)} \rangle$	$\langle g^{(\parallel)} \rangle$	$ \langle g^{(\perp)} - \langle g^{(\perp)} \rangle  $	$ \langle g^{(\parallel)} - \langle g^{(\parallel)} \rangle  $
Period 1	-1.223	-6.307	0.4769	5.142
Period 2	-3	-7.767	1.678	10.30
SBR	-3	-7.038	1.714	7.856

TABLE V. Results of numerical tests on the Ott–Sommerer system. In this table F implies that this type of driving fails the test. For off-diagonal driving the first number listed is either  $\epsilon_1$  or  $\epsilon_2$  while the number listed below it is either  $\epsilon_3$  or  $\epsilon_4$ .

Drive measure	Drive type	Ott–Sommerer system					
		Rigorous tests		Approximate test		Numerical test	
		$\perp$	$\parallel$	$\perp$	$\parallel$	$\perp$	$\parallel$
Period 1	Diagonal all	0.812	4.04	0	0	0.01	0.28
	Diagonal only $x$	F	F	0	0	0.01	0.62
	Diagonal only $v$	F	F	0	0	0.01	0.69
	Off-Diagonal $x$	0.95 0	0.95 99.6	0 0	0 0	0.002 0.04	0.15 0.55
Period 2	Diagonal all	1.89	7.34	0	0	0.13	0.99
	Diagonal only $x$	F	F	0	0	0.25	2.6
	Diagonal only $v$	F	F	0	0	0.24	2.8
	Off-Diagonal $x$	0.95 8.47	0.95 416	0 0	0 0	0.05 0.9	0.5 1.75
SBR	Diagonal all	1.92	5.87	0	0	0.05	0.52
	Diagonal only $x$	F	F	0	0	0.09	1.9
	Diagonal only $v$	F	F	0	0	0.10	1.5
	Off-Diagonal $x$	0.95 8.95	0.95 193	0 0	0 0	0.05 0.7	0.5 1.75

plifies the guaranteed synchronization condition (this is the form used to generate the numerical values shown in Table V)

$$\epsilon_1 > 1 - \nu,$$

$$\epsilon_3 = \frac{1}{4}(\nu - \epsilon_1)^2 + [\langle g \rangle + 4\langle |g - \langle g \rangle| \rangle]^2.$$

### 3. Driving via velocity

This type of driving uses only the velocity variables,  $v_x$  and  $v_y$ . As an example, let the velocity variables drive both the position and the velocity equations. Thus,  $\epsilon_1 = \epsilon_3 = 0$  and the parameter space is  $\mathbb{R}^2$ . Again we notice that if Eq. (18) is satisfied, then  $\Lambda_{\pm}$  are complex. However, even if Eq. (18) is satisfied, values of  $\epsilon_2$  and  $\epsilon_4$  which satisfy the rigorous condition for synchronization do not exist. To see this define new parameters  $u \equiv \nu + \epsilon_2$  and  $w \equiv (\epsilon_4 - 1)/C$ . In terms of the new parameters, Eqs. (17) and (18) are

$$u > 4C\langle |g - \langle g \rangle| \rangle,$$

$$(2C\langle g \rangle)^2 = u^2 + (2C\langle g \rangle - w)^2,$$

where  $C$  is arbitrary. These equations define a line and a circle, respectively. It is straightforward to show that the circle does not intersect the line on the measures we have examined. Therefore, the rigorous condition for synchronization can not be satisfied by this type of driving.

## V. SUMMARY

In this paper we investigated the linear stability of the invariant manifold associated with synchronous behavior between coupled dynamical systems. (See Appendix B for a discussion of these manifolds.) Although we examined a particular type of coupling, our results are valid for more gen-

eral types of coupling, and they can be used to determine the linear stability of invariant manifolds within a dynamical system (see Appendix A).

We have two major results. The first is a rigorous criterion, given by Eqs. (8)–(10). If it is satisfied, then linear stability of synchronization to the driving trajectory is guaranteed. The condition is based on norms of deviations from synchronous behavior. As such it tends to overestimate the coupling strength needed to achieve synchronization. (An alternative formulation of the rigorous criteria can be found in Appendix E.) The second result, given by Eq. (12), is a “quick and dirty” criterion for estimating the coupling strengths needed to produce synchronous behavior. The approximation is easy to calculate and can be used to quickly investigate many coupling schemes and strengths. A major advantage to our approach is that both the rigorous and approximate criterion have a geometric interpretation that can be used to design couplings schemes and strengths that will result in synchronization (see Appendix C). Both criterion can also be related to fundamental issues in control theory (see Appendix D).

Both the rigorous and approximate condition are dependent on the measure used for the driving dynamics and can yield different stability results for different driving trajectories. Nonetheless, based on our results, and previous work by others, it may be possible to design couplings that result in linearly stable synchronization for arbitrary driving trajectories.<sup>28</sup>

To test these criteria we have performed numerical experiments on four different dynamical systems, the Rossler, Lorenz (see also Appendix E), and Ott–Sommerer systems and a system used to model chaotic masking in communication (see Appendix A). When taken together, these examples provide a thorough examination of the stability criterion we propose.

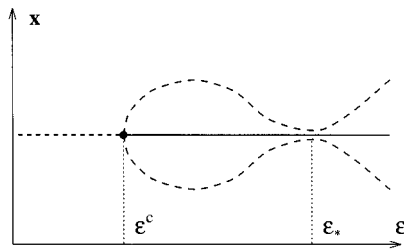


FIG. 9. An example of a possible bifurcation diagram for the stability of synchronization onto an unstable fixed point. If the coupling parameter has a value near either  $\epsilon^{(c)}$  or  $\epsilon_*$ , then it is likely that noise will cause the response system flip beyond the unstable solution and away from the synchronization manifold.

We close with a discussion of how noise and nonlinear effects influence the conclusions one can draw from the linear stability analysis. In this context consider a chaotic attractor that contains an unstable fixed point at  $\mathbf{x}=\mathbf{0}$ . Furthermore, assume that  $\mathbf{x}=\mathbf{0}$  is the driving trajectory, and the response system synchronizes onto this fixed point as the coupling strength increases. The change in stability as  $\epsilon$  increases is a bifurcation which we will model by a pitchfork (see Fig. 9). A linear stability analysis does not take into account the existence of the unstable trajectories for  $\epsilon > \epsilon^{(c)}$ . For arbitrarily small noise amplitude there exists a range of  $\epsilon$  values near  $\epsilon^{(c)}$  where noise will eventually push the response system above or below the dashed lines. When this occurs the response system can not collapse back to the synchronized state and is forced to seek out an attracting state away from the synchronization manifold. Also, a linear stability analysis does not take into account the existence of the unstable trajectories near  $\mathbf{x}=\mathbf{0}$  when  $\epsilon \approx \epsilon_*$ . If  $\epsilon \approx \epsilon_*$ , then noise may cause a loss of synchronization. Therefore, although a linear stability analysis may seem to guarantee stable synchronous motion, noise and nonlinear effects may prevent long term synchronous behavior.

**ACKNOWLEDGMENTS**

The authors would like to thank Alistair Mees, David Walker, Dan Gauthier, Bill Helton, and Lou Pecora for graciously providing encouragement and advice during the performance of this work. The authors would like to thank Lev Tsimring and Doug Ridgway for helpful discussions. R. Brown was supported by the Office of Naval Research, Grant No. N00014-95-1-0864 and the Air Force Office of Scientific Research, Grant No. F49620-95-1-0261. N. Rulkov was supported the U.S. Department of Energy, Grant No. DE-FG03-95ER14516.

**APPENDIX A: RELATED PROBLEMS**

With minor modifications the techniques and results discussed above are valid for more general types of coupling. They can also be used to study the stability of invariant manifolds of a dynamical system. In part, this generality exists because the linearized stability equations we examine arise in a variety of other problems, many of which have

recently appeared in the literature. The key point to realize is that a linearized equation, similar to Eq. (3), arises whenever a dynamical system has dynamics on a smooth invariant manifold of its full phase space, and one is considering the linear stability of this manifold to perturbations which are transverse to the manifold.

For example, the equations examined by Ott–Sommerer are of the form

$$\frac{d\mathbf{x}}{dt} = \mathbf{F}(\mathbf{x}, \mathbf{y}; t),$$

$$\frac{d\mathbf{y}}{dt} = \mathbf{M}(\mathbf{x}, \mathbf{y}; t)\mathbf{y},$$

where  $\mathbf{M}$  is an  $n \times n$  matrix whose elements are functions of  $\mathbf{x} \in \mathbb{R}^m$  and  $\mathbf{y} \in \mathbb{R}^n$  and time,  $t$ . For this system  $\mathbf{y}=\mathbf{0}$  is an invariant manifold. The linearized equations of motion for  $\mathbf{w}=\mathbf{y}-\mathbf{0}$  are the same as Eq. (15) with  $\mathbf{DE}^{(\perp)}=\mathbf{0}$  [see Eqs. (7) and (8) in Ref. 21]. If this manifold is unstable, then one can use our criterion to determine a  $\mathbf{DE}^{(\perp)}$  that stabilizes this manifold. By absorbing  $\mathbf{DE}^{(\perp)}$  into the matrix  $\mathbf{M}(\mathbf{x}, \mathbf{y}; t)$  one can determine values for the parameters in  $\mathbf{M}$  that yield a linearly stable invariant manifold.

Another type of problem that is covered by our formalism is synchronization between mutually coupled identical systems. The equations of motion for this problem are often of the form

$$\frac{d\mathbf{x}}{dt} = \mathbf{F}(\mathbf{x}) + \mathbf{E}_1(\mathbf{y} - \mathbf{x}),$$

$$\frac{d\mathbf{y}}{dt} = \mathbf{F}(\mathbf{y}) + \mathbf{E}_2(\mathbf{x} - \mathbf{y}),$$

where  $\mathbf{E}_1$  and  $\mathbf{E}_2$  are functions of their argument and  $\mathbf{E}_1(\mathbf{0})=\mathbf{E}_2(\mathbf{0})=\mathbf{0}$ . Because of the lack of constant terms in  $\mathbf{E}_1$  and  $\mathbf{E}_2$  the synchronization manifold  $\mathbf{x}=\mathbf{y}$  is invariant. The linear stability of this manifold is determined by Eq. (3) where  $\mathbf{DE}(\mathbf{0})=\mathbf{DE}_1(\mathbf{0})+\mathbf{DE}_2(\mathbf{0})$ . Using our criterion to determine an  $\mathbf{E}$  that results in linearly stable synchronization is equivalent to determining forms for  $\mathbf{E}_1$  and  $\mathbf{E}_2$ . (Here, the nonuniqueness of the decomposition  $\mathbf{DE}=\mathbf{DE}_1+\mathbf{DE}_2$  can probably be reconciled using details of the specific problem under investigation.)

Finally, synchronization in drive response systems of the form

$$\frac{d\mathbf{x}}{dt} = \mathbf{F}(\mathbf{x}),$$

$$\frac{d\mathbf{y}}{dt} = \mathbf{G}(\mathbf{y}, \mathbf{x}; \epsilon),$$

where  $\mathbf{F}=\mathbf{G}$  when  $\mathbf{x}=\mathbf{y}$  and/or  $\epsilon=1$ , has been previously examined.<sup>23,32,33</sup> For this system  $\mathbf{x}=\mathbf{y}$  is an invariant manifold for all values of  $\epsilon$ . (We present an example of this type of system below.)

For each of these problems the important research issues center around the stability of an invariant manifold of the dynamics. In particular, synchronization between  $N$  coupled

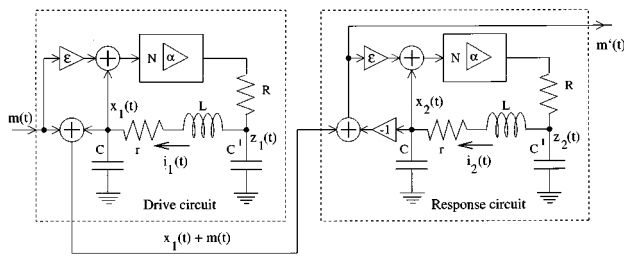


FIG. 10. A block diagram of electronic circuits that are modeled by Eqs. (A1) and (A4).

dynamical systems can often be thought of as motion on a smooth invariant manifold which lives in the full phase space of a single large dynamical system consisting of the  $N$  smaller systems. Given this interpretation, our results indicate that the stability of synchronization is a special case of the stability of invariant manifolds of a dynamical system. (A similar observation can be found in Ref. 14.) Therefore, although our results are presented in the context of synchronization between identical chaotic systems coupled in a drive/response manner, they are applicable to areas of research where the stability of invariant manifolds is the central issue. Examples of this are riddled basins and on-off intermittency, synchronization of identical systems with mutual coupling, and generalized synchronization.<sup>14,21,32–36</sup>

### 1. Communication example

This example is a modification of a synchronization method which has previously been used to experimentally demonstrate communication via modulated chaotic signals.<sup>32</sup> The modification involves introducing a parameter,  $\epsilon$ , whose variation changes the stability properties of the synchronization manifold. Introducing this additional parameter, and carefully selecting its value, can enhance the stability of the synchronization manifold.<sup>19,23</sup> Therefore, adding this parameter is very useful for applications.

A block diagram of the modified drive and response circuits is shown in Fig. 10. Each circuit consists of a nonlinear converter,  $N$ , which transforms input voltage,  $u$ , into output,  $\alpha f(u)$  (see Ref. 12 for details). The parameter  $\alpha$  characterizes the gain of  $N$  around  $x=0$ . The nonlinear amplifier has linear feedback which contains a series connection to a low-pass filter,  $RC'$ , and a resonant circuit  $LC$ .

Our analysis requires knowledge of the equations of motion for the systems. The dynamics of the chaotic driving circuit can be described by the following system of three ODE's

$$\begin{aligned} \frac{dx_1}{dt} &= y_1, \\ \frac{dy_1}{dt} &= -x_1 - \delta y_1 + z_1, \\ \frac{dz_1}{dt} &= \gamma[\alpha f(x_1 + \epsilon m) - z_1] - \sigma y_1, \end{aligned} \tag{A1}$$

where the parameters  $\alpha$ ,  $\gamma$ ,  $\delta$ ,  $\epsilon$  and  $\sigma$  are all positive. (The relations between the parameters of the model and the parameters of the circuits can be found in Ref. 12). In these equations  $m$  denotes the time dependent message one wants to send, although  $x_1 + m$  is the actual transmitted signal.

In numerical simulations we use

$$\begin{aligned} f(x) &= -\text{sign}(x) \left( \frac{a}{a-c} \right) \\ &\times \left( -a + \left[ \left( \frac{a^2-c}{a^2} \right) (f_1(x) - a)^2 + c \right]^{1/2} \right), \end{aligned} \tag{A2}$$

where

$$f_1(x) = \begin{cases} |x|, & \text{if } |x| \leq a, \\ -a[2|x| - (b+a)] / (b-a), & \text{if } a < |x| \leq b, \\ -a, & \text{if } |x| > b. \end{cases} \tag{A3}$$

If we set  $a=0.5$ ,  $b=1.8$  and  $c=0.03$ , then  $f(x)$ , as given by Eqs. (A2) and (A3), fits the nonlinearity of the converter,  $N$ , to within  $\approx 2\%$  accuracy. The validity of the model (A1)–(A3) has been confirmed via synchronization between the real circuit and the model.<sup>3</sup>

The response system is driven by the voltage  $x_1$  from the drive system. Experimentally, it is fed into another circuit which couples it to the transmitted signal,  $x_1 + m$  (see Fig. 10). The dynamics of the response circuit is

$$\begin{aligned} \frac{dx_2}{dt} &= y_2, \\ \frac{dy_2}{dt} &= -x_2 - \delta y_2 + z_2, \\ \frac{dz_2}{dt} &= \gamma[\alpha f(x_2 + \epsilon(x_1 + m - x_2)) - z_2] - \sigma y_2. \end{aligned} \tag{A4}$$

The parameter,  $\epsilon$ , indicates the strength of the coupling between the drive and response circuit. Note that if  $\epsilon=0$ , then the drive and response system are uncoupled. If  $\epsilon=1$ , then a driving signal,  $x_1 + m$ , is the argument of the nonlinearity of the response circuit. If the drive and response circuit synchronize, then the response system operates as a ‘‘chaos filter’’ which can be used to extract the message from the transmitted signal. (To see this, notice that if  $\epsilon=1$ , and the response system synchronizes to the drive system, then  $x_2=x_1$  and the message,  $m$ , can be recovered by subtracting  $x_2$  from transmitted signal.) More importantly for applications, if the two systems synchronize for  $\epsilon \neq 1$ , then this same procedure can still be used to transmit messages.

An examination of Eqs. (A1) and (A4) results in the following equations for **A** and **B**:

$$\mathbf{A} = \begin{bmatrix} 0 & -1 & 0 \\ -1 & -\delta & 1 \\ 0 & -\sigma & \gamma \end{bmatrix},$$

and

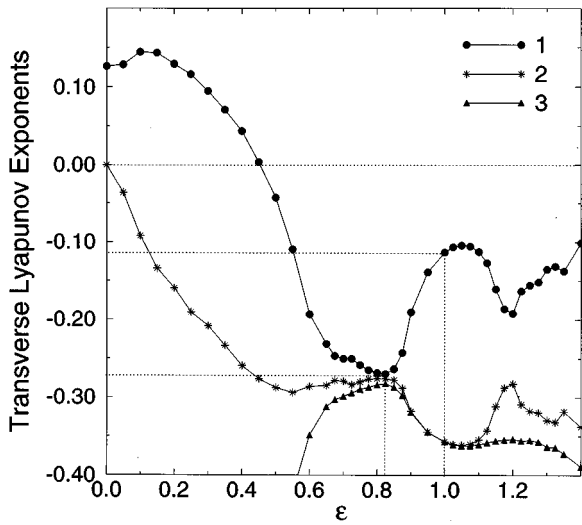


FIG. 11. The transverse Lyapunov exponents as a function of  $\epsilon$ .

$$\mathbf{B}(\mathbf{x}_1) = \begin{bmatrix} 0 & 0 & 0 \\ 0 & 0 & 0 \\ g(\mathbf{x}_1) & 0 & 0 \end{bmatrix},$$

where  $g(\mathbf{x}_1) = \alpha\gamma(1 - \epsilon)f'(x_1 + m)$  and  $f'(x) \equiv df(x)/dx$ . The characteristic equation for  $\mathbf{A}$  is

$$\Lambda^3 + (\delta + \gamma)\Lambda^2 + (1 + \sigma + \gamma\delta)\Lambda + \gamma = 0.$$

This equation is not easily solved for the eigenvalues. However, the Routh Hurwitz criteria indicates that  $\Re[\Lambda] < 0$  for all eigenvalues.<sup>37</sup>

For this example,  $\mathbf{A}$  is independent of  $\epsilon$  and  $\langle \|\mathbf{P}^{-1}[\mathbf{B}(\mathbf{x})]\mathbf{P}\| \rangle = 0$  when  $\epsilon = 1$ . Therefore, if  $\epsilon = 1$ , then the rigorous condition for linear stability of the synchronization manifold ( $\Re[\Lambda_1] < 0$ ) is satisfied. If  $\epsilon \neq 1$ , then  $\langle \|\mathbf{P}^{-1}[\mathbf{B}(\mathbf{x})]\mathbf{P}\| \rangle \neq 0$  and this simple analysis fails.

To understand the importance of  $\epsilon \neq 1$  for applications notice that if  $f(x)$  is given by Eqs. (A2) and (A3), then  $f'(x)$  is not continuous. However, this function is only an approximation to the real  $f(x)$ . If the real  $f(x)$  has a continuous derivative (in fact we believe  $f(x)$  is smooth), then there exists an open neighborhood of  $\epsilon = 1$  where the rigorous condition for synchronization [Eq. (10)] is guaranteed to be satisfied.

The existence of this neighborhood is important because, although the synchronization manifold is linearly stable for  $\epsilon = 1$ , this does not guarantee that  $\epsilon = 1$  results in the *most* stable manifold. The loss of synchronization is unfavorable for applications involving communications. Thus, one wants a synchronization manifold that is as stable as possible, and which recaptures the response trajectory as soon as possible in the event that synchronization is lost. Therefore, one should to use an  $\epsilon$  value that yields the *most stable* synchronization manifold.

In Fig. 11 we show the transverse Lyapunov exponents as a function of  $\epsilon$  for our model. The figure indicates that, at least as far as transverse Lyapunov exponents are concerned,

the most stable synchronization manifold occurs when  $\epsilon \neq 1$ . The fact that the rigorous condition is guaranteed to be satisfied in some neighborhood of  $\epsilon = 1$  means that we are free to search for values of  $\epsilon$  that result in the most stable synchronization manifold.

### APPENDIX B: GEOMETRICAL DISCUSSION OF INVARIANT MANIFOLDS

In this appendix we discuss the various invariant manifolds that arise when discussing synchronization. The idea of an invariant manifold is fundamental to our approach. Because we have discussed many different invariant manifolds it is useful to carefully construct a geometric picture of these manifolds. This construction provides a unified interpretation of the issues discussed above. Let  $\mathbf{x} \in \mathbb{R}^d$  denote the trajectory of the driving system and let  $\mathbf{y} \in \mathbb{R}^d$  denote the trajectory of the response system. Hence, the full phase space that describes the evolution of the two systems is  $\mathbb{R}^{2d}$ . If  $\mathbf{z}$  denotes a trajectory in the full phase space, then the synchronization manifold for identical systems is defined by  $\mathcal{W}^s \equiv \{\mathbf{z} = (\mathbf{x}, \mathbf{y}) | \mathbf{x} = \mathbf{y}\}$ .

Next, assume that the driving trajectory evolves on an  $m \leq d$  dimensional invariant manifold,  $\mathcal{W}_D$ . This manifold may, or may not, be stable to perturbations. For example, if the driving trajectory is an unstable fixed point, then  $m = 0$ , and  $\mathcal{W}_D$  is unstable. If the driving trajectory is an unstable limit cycle, then  $m = 1$ , and  $\mathcal{W}_D$  is unstable. However, if the driving trajectory is a dense orbit on a chaotic attractor, then  $m \leq d$  and  $\mathcal{W}_D$  is stable. (For this case we are not saying that  $\mathcal{W}_D$  is the attractor. Rather,  $\mathcal{W}_D$  is the manifold that contains the attractor.) For all of these cases it is possible for  $\mathcal{W}_D$  to occupy zero volume in  $\mathbb{R}^d$ . Finally, if the system is Hamiltonian and the driving trajectory is chaotic, then  $m = d$  and  $\mathcal{W}_D$  occupies positive volume in  $\mathbb{R}^d$ .

In addition, the dynamical system itself may have an invariant manifold,  $\mathcal{W}^0 \subset \mathbb{R}^d$  (which we call an invariant manifold of the system). An invariant manifold of the system may contain an infinite number of trajectories. For example, the Ott–Sommerer system discussed above has an invariant manifold defined by  $y = v_y = 0$ , and a chaotic attractor exists in this manifold.<sup>21</sup> (This chaotic set is attracting for points within the manifold defined by  $y = v_y = 0$ .) Therefore, it is possible to consider a case where  $\mathcal{W}_D$  is restricted to an invariant manifold of the system,  $\mathcal{W}_D \subseteq \mathcal{W}^0$ . However, in general this is not the case. An important point to keep in mind is that the driving trajectory defines  $\mathcal{W}_D$ , and each different driving trajectory (in general) defines a different  $\mathcal{W}_D$ .

For identical systems, the response system has an identical  $m$  dimensional manifold,  $\mathcal{W}_R$ . The manifolds  $\mathcal{W}_D$  and  $\mathcal{W}_R$  are not the same because  $\mathcal{W}_D$  lives in the phase space of the driving system while  $\mathcal{W}_R$  lives in the phase space of the response system.

In the full phase space of the combined system these manifolds can be defined by  $\mathcal{W}_D^* \equiv \{\mathbf{z} = (\mathbf{x}, \mathbf{y}) | \mathbf{x} \in \mathcal{W}_D\}$ , and  $\mathcal{W}_R^* \equiv \{\mathbf{z} = (\mathbf{x}, \mathbf{y}) | \mathbf{y} \in \mathcal{W}_R\}$ . (See Fig. 12 for a schematic picture of these manifolds.) These manifolds intersect in the full

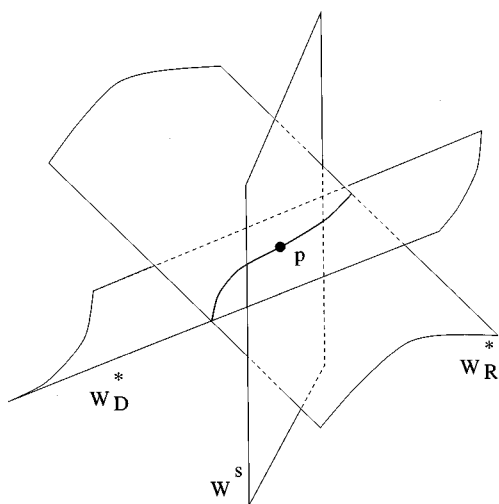


FIG. 12. Various manifolds and intersections which arise in the phase space associated with two identical systems which are coupled together.

phase space. The intersection is defined by  $\mathcal{W}_D^* \cap \mathcal{W}_R^* \equiv \{z = (x, y) | x \in \mathcal{W}_D \text{ and } y \in \mathcal{W}_R\}$  (see the dark solid curve in Fig. 12). Since this definition does not require  $x = y$ , it is clear that, although  $\mathcal{W}_D^* \cap \mathcal{W}_R^*$  contains part of the synchronization manifold,  $\mathcal{W}_D^* \cap \mathcal{W}_R^* \neq \mathcal{W}^s$ . Furthermore,  $\mathcal{W}^s$  contains all possible driving trajectories. Therefore, if  $\mathcal{W}_D$  is restricted to an invariant manifold of the system ( $\mathcal{W}_D \subseteq \mathcal{W}^0$ ), then some trajectories within  $\mathcal{W}^s$  are not in  $\mathcal{W}_D^*$ .

Therefore, when we discuss the linear stability of synchronization for a given driving trajectory we are actually discussing the stability of the manifold given by  $\mathcal{W} \equiv \mathcal{W}_D^* \cap \mathcal{W}_R^* \cap \mathcal{W}^s \equiv \{z = (x, y) | x \in \mathcal{W}_D^* \text{ and } y \in \mathcal{W}_R^* \text{ and } x = y\}$  to perturbations that are transverse to this manifold. The manifold associated with this intersection is labeled  $p$  in Fig. 12. Although it is shown as a dot one must keep in mind that the dimension of the manifold,  $\mathcal{W}$ , ranges from a low of zero to a high of  $d$ . If  $\mathcal{W}_D^* \cap \mathcal{W}_R^* \cap \mathcal{W}^s$  is stable for all possible driving trajectories we say that  $\mathcal{W}^s$  is stable.

**APPENDIX C: GEOMETRICAL INTERPRETATION OF THE STABILITY CRITERIA**

In this appendix we discuss a geometrical interpretation of the stability criteria discussed in Sections II and III. Equations (10) and (12) have geometrical interpretations which can be used to design couplings that yield stable synchronous motion. One can think of the elements of  $DE(0)$  as living in a  $d^2$  dimensional parameter space. The right hand side of Eq. (10) defines a function in this parameter space. Furthermore, this function can be used to define a family of surfaces in this parameter space. Explicitly, the family of surfaces  $\Sigma_B$  is defined by  $\langle \|P^{-1}[B(x;t)P]\rangle = C_B$ , where  $C_B$  is a constant. In a similar fashion the left hand side defines a different function and family of surfaces. Explicitly, the family of surfaces  $\Sigma_A$  is defined by  $-\Re[\Lambda_1] = C_A$ , where  $C_A$  is a constant.

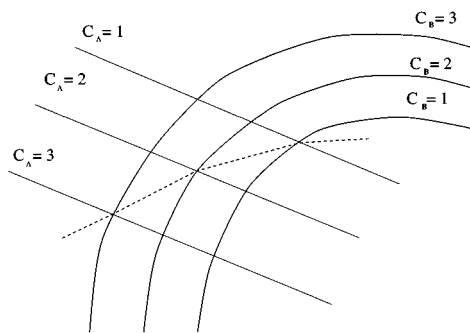


FIG. 13. Various surfaces  $\Sigma_A$  and  $\Sigma_B$ . The dashed line is the boundary of the region of parameter space that yields linearly stable synchronization. Any location in parameter space “above” this line will yield linearly stable synchronization.

Now consider a fixed driving trajectory. For this trajectory, each value of  $C_B$  ( $C_A$ ) corresponds to a particular surface from the family  $\Sigma_B$  ( $\Sigma_A$ ). The boundary of the region of parameter space that yields linearly stable synchronization is given by the intersections of surfaces from  $\Sigma_A$  with surfaces from  $\Sigma_B$  where  $C_B = C_A$ . These intersections form a surface in the parameter space. Any intersection associated with  $C_A > C_B$  will result in linearly stable synchronization onto the driving trajectory. Furthermore, all of these intersections will reside on one side of the surface defined by the boundary (see Fig. 13). Because  $C_A$  and  $C_B$  are (in general) arbitrary real numbers, and the reals are dense, we know that the region associated with linearly stable synchronization will typically occupy positive volume in the phase space.

An immediate consequence of this approach is that if none of the surfaces from  $\Sigma_A$  intersect surfaces from  $\Sigma_B$ , then the rigorous criterion for synchronization can not be met.

An explicit example of this analysis is the Ott-Sommerer example discussed above. For this example Eqs. (17) and (18) are equivalent to the stability criterion of Eq. (10). Begin with the diagonal driving example and consider a fixed driving trajectory. For this example the parameter space is  $\mathbb{R}$  and  $C$  [from Eq. (18)] is a constant, independent of  $\epsilon$ . Because  $C$  is constant,  $C_B$  can have only one value and there is only one surface in the family  $\Sigma_B$ . Furthermore, the fact that the right hand side of Eq. (17) is independent of  $\epsilon$  implies that  $\Sigma_B$  is the entire parameter space. In contrast  $C_A$  can take on any value. The left hand side of Eq. (17) indicates that a particular value of  $C_A$  corresponds to a particular value of  $\epsilon$ . Therefore,  $\Sigma_A$  is a family of points in the parameter space  $\mathbb{R}$ .

For these surfaces the boundary of the region of parameter space that yields linearly stable synchronization (the intersection of  $\Sigma_A$  and  $\Sigma_B$  associated with  $C_A = C_B$ ) is a point in  $\mathbb{R}$ . Intersections associated with  $C_A > C_B$  are also points. Finally, the region associated with linearly stable synchronization (the intersection of all surfaces from  $\Sigma_A$  with surfaces from  $\Sigma_B$  such that  $C_A > C_B$ ) is an interval which occupies positive volume in  $\mathbb{R}$  [see Eq. (19)].

The final example is driving with position, and the posi-

tion is permitted to drive both the position and velocity equations. The parameter space for this example is  $\mathbb{R}^2$ . Now, assume the driving trajectory is fixed. The derivation that lead to Eq. (21) shows that  $\Sigma_{\mathbf{B}}$  is a family of parabolas in  $\mathbb{R}^2$ . Selecting a value for  $C_{\mathbf{B}}$  is equivalent to selecting a value for  $C$ , which is equivalent to selecting a particular parabola from this family.

The left hand side of Eq. (17) indicates that  $\Sigma_{\Lambda}$  is a family of lines in  $\mathbb{R}^2$ . Selecting a value for  $C_{\Lambda}$  selects a particular line from this family. Thus, if one has chosen a particular value for  $C$ , then the boundary of the parameter space region that yields stable synchronization is the intersection of a line and a parabola. For this example this intersection always exists. Intersections of lines associated with  $C_{\Lambda} > C_{\mathbf{B}}$  (for fixed  $C$ ) sweep out a portion of the parabola. Therefore, for fixed  $C_{\mathbf{B}}$  (equivalently, fixed  $C$ ) the portion of the parabola that is beyond the line associated with  $C_{\Lambda} = C_{\mathbf{B}}$  corresponds to values of the coupling parameters that produce stable synchronous motion.

Now recall that the value of  $C$  is arbitrary, and different values of  $C$  yield different parabolas. For each different value of  $C$  the rigorous criterion chooses a portion of a parabola. Therefore, the region of parameter space that satisfies the rigorous criterion is the one swept out by portions of the parabolas for all possible values of  $C$ . This region occupies positive volume in the parameter space,  $\mathbb{R}^2$ .

#### APPENDIX D: RELATIONSHIP TO CONTROL THEORY

In this appendix we discuss the relationship between our results and those found in control theory. The relationship between synchronization and control has been known for some time.<sup>38,39</sup> In these papers synchronization is typically discussed as an example of feedback control (see the review by Chen and Dong<sup>9</sup>).

In basic control theory one is often interested in the following equation:

$$\frac{d\mathbf{w}}{dt} = \hat{\mathbf{A}}(t)\mathbf{w} + \hat{\mathbf{B}}(t)u(t),$$

where  $u(t)$  is a time dependent scalar input (the drive). In this equation we are invited to think of  $\hat{\mathbf{A}}$  as the uncontrolled dynamics and  $\hat{\mathbf{B}}(t)$  as a matrix which couples the input to the uncontrolled dynamics. An important question in control theory is, can one find inputs,  $u(t)$ , so that the  $\mathbf{w}(t) = \mathbf{0}$  in finite time. The answer to this question is often determined by constructing a controllability matrix

$$G(t, t_0) = \int_{t_0}^t \mathbf{U}(t, s) \hat{\mathbf{B}}(s) \hat{\mathbf{B}}^\dagger(s) \mathbf{U}^\dagger(t, s) ds, \quad (\text{D1})$$

where  $\mathbf{U}(t, t_0) = \exp[\int_{t_0}^t \mathbf{A}(s) ds]$ . It is known that if  $G(t, t_0)$  has full rank ( $\det(G) \neq 0$ ), then one can find inputs so that  $\mathbf{w}(t) = \mathbf{0}$ .<sup>31</sup>

We are interested in the following linearized equation of motion:

$$\frac{d\mathbf{w}}{dt} = [\mathbf{DF}(t) + \mathbf{DE}(\mathbf{0})]\mathbf{w}.$$

For the coupling we have considered the inputs are feedbacks,  $u(t) = \sum_{\alpha=1}^d \hat{C}_{\alpha} w_{\alpha}$  where  $\hat{C}$  is a constant vector (which typically has only one component). Therefore, a controllability approach would involve determining a  $\hat{\mathbf{B}}$  so that  $G(t, t_0)$  has full rank and then using  $DE(\mathbf{0})_{\alpha\beta} = \hat{B}_{\alpha} \hat{C}_{\beta}$  to obtain  $\mathbf{DE}(\mathbf{0})$ .

The difficulty with the controllability approach is that  $\mathbf{U}(t, t_0)$  has a complicated time dependence. Avoiding this complication is one of the motivations for considering the equation

$$\frac{d\mathbf{w}}{dt} = [\mathbf{A} + \mathbf{B}(t)]\mathbf{w}, \quad (\text{D2})$$

where  $\mathbf{A}$  and  $\mathbf{B}$  are defined by Eqs. (8) and (9). In this formulation of the problem the coupling strengths ( $\mathbf{DE}(\mathbf{0})$ ) are part of  $\mathbf{A}$ , we think of  $\mathbf{A}$  as the uncontrolled dynamics, and  $\mathbf{B}(t)\mathbf{w}$  are driving inputs. In effect the rigorous criterion of Eq. (10) says that if the eigenvalues of  $\mathbf{A}$  are placed sufficiently far into the right half-plane (as a result of feedback coupling) then the fluctuation that result from the chaotic driving are not sufficient to destabilize the fixed point at  $\mathbf{w} = \mathbf{0}$ . In this sense our criterion is similar in spirit to pole placement control theory.

We remark that the controllability matrix can not be immediately calculated for Eq. (D2) because  $\hat{\mathbf{B}}$  is a function that maps input space into state space while  $\mathbf{B}$  is a function that maps state space into itself. In Eq. (D2) the function that plays the role of  $\hat{\mathbf{B}}$  is part of the matrix  $\mathbf{A}$ .

We believe that a different interpretation of synchronization (still from control theory) could be quite promising. Walker and Mees interpret synchronization as an example of state estimation and the observer problem.<sup>18</sup> This view of synchronization says that synchronization permits one to estimate the complete state of a system when the full state vector is not observable. In practice one could imagine coupling the output from a physical system to a model of the system using coupling that is guaranteed to result in stable synchronization. (Here we rely on the fact that synchronization is robust to modeling errors and noise.<sup>3</sup>) The full state of the physical system is then the same as the state of the model. For the linear system the observer problem and the control problem can be shown to be duals of each other.<sup>40,31</sup> Thus, many of the results proved for observability of a dynamical system are corollaries of theorems proved for control. In this paper a rigorous and easy to calculate criterion for synchronization is given.

#### APPENDIX E: ANOTHER RIGOROUS CRITERION

In this appendix we describe a derivation that leads to a rigorous criterion similar to the one derived in Section II. If one does not transform to coordinates given by the eigenvectors of  $\mathbf{A}$ , then Eq. (5) becomes

$$\mathbf{w}(t) = \mathbf{U}(t, t_0)\mathbf{w}(t_0) + \int_{t_0}^t \mathbf{U}(t, s)\mathbf{B}(s)\mathbf{w}(s)ds,$$

where  $\mathbf{U}(t, t_0) = \exp[\mathbf{A}(t - t_0)]$ . This equation leads to Eq. (6) as a sufficient condition for linear stability of synchronization with  $\mathbf{K}$  replaced by  $\mathbf{B}$ . It is straightforward to show if  $\mathbf{U}(t, t_0) = \exp[\mathbf{A}(t - t_0)]$ , then a rigorous sufficient condition for linear stability of synchronization is

$$-\Re[\Lambda_{\pm}] > C\langle \|\mathbf{B}\| \rangle, \tag{E1}$$

where

$$C = \left[ \sum_{\alpha\beta} \left| P_{\alpha 1} P_{1\beta}^{-1} \right|^2 \right]^{1/2}. \tag{E2}$$

For this criterion the terms involving the coupling strength and the time average have been decoupled. This could greatly simplify the effort required for some calculations.

As an example consider the Lorenz system. The eigenvectors of  $\mathbf{A}$  are

$$\hat{\mathbf{e}}_z = \hat{\mathbf{z}},$$

$$\hat{\mathbf{e}}_{\pm} = \frac{1}{N_{\pm}} [(\sigma - \epsilon_4), (\sigma + \epsilon_1 + \Lambda_{\pm}), 0],$$

where  $N_{\pm}$  are the following normalizations:

$$N_{\pm} = [(\sigma - \epsilon_4)^2 + |\sigma + \epsilon_1 + \Lambda_{\pm}|^2]^{1/2}.$$

Also,  $\mathbf{B}(\mathbf{x})$  is given by

$$\mathbf{B}(\mathbf{x}) = \begin{bmatrix} 0 & 0 & 0 \\ -z + \langle z \rangle & 0 & -x + \langle x \rangle \\ y - \langle y \rangle & x - \langle x \rangle & 0 \end{bmatrix}.$$

Clearly, calculating  $\|\mathbf{P}^{-1}\mathbf{B}(\mathbf{x})\mathbf{P}\|$  is a complicated procedure. However, the rigorous condition of Eq. (E1) can be easily satisfied. It is possible to show that if  $\Lambda_{\pm}$  are complex, then

$$C = \left[ \frac{(r - \langle z \rangle - \epsilon_3 + 1)^2}{-[\sigma + \epsilon_1 - 1 - \epsilon_2]^2 - 4(r - \langle z \rangle - \epsilon_3)(\sigma - \epsilon_4)} \right]^{1/2}.$$

Now consider off-diagonal  $y$ -driving ( $\epsilon_1 = \epsilon_3 = 0$ ) and fixed  $C$ . To satisfy the rigorous condition of Eq. (E1) while keeping  $C$  fixed one needs

$$\epsilon_2 > -(\sigma + 1) + 4C\langle \|\mathbf{B}\| \rangle,$$

$$\epsilon_4 = \frac{(\epsilon_2 + 1 - \sigma)^2}{4(r - \langle z \rangle)} + \left[ \sigma + \frac{(r - \langle z \rangle - 1)^2}{4C^2(r - \langle z \rangle)} \right],$$

where  $C$  is arbitrary. The second equation is a parabola which exists for all values of  $\epsilon_2$ , and all driving trajectories. The first equation is a line which is guaranteed to intersect the parabola. Therefore the rigorous condition of Eq. (E1) can be satisfied for this type of driving.

<sup>1</sup>H. Fujisaka and T. Yamada, *Prog. Theor. Phys.* **69**, 32 (1983).  
<sup>2</sup>T. P. Carroll and L.M. Pecora, in *Nonlinear Dynamics in Circuits*, edited by T. L. Carroll and L. M. Pecora (World Scientific, Singapore, 1995).  
<sup>3</sup>R. Brown, N. F. Rulkov, and N. B. Tufillaro, *Phys. Rev. E* **50**, 4488 (1994).  
<sup>4</sup>L. M. Pecora, *Chaos in Communications, SPIE Proceedings, San Diego, CA, 1993*, **2038** (SPIE-The International Society for Optical Engineering, Bellingham, WA), pp. 2–25 (1993).  
<sup>5</sup>U. Feldmann, ‘‘Synchronization of Chaotic Systems,’’ Ph.D. dissertation, Faculty of Electrical Engineering, Technical University of Dresden, July 1995.  
<sup>6</sup>N. F. Rulkov, M. M. Sushchik, L. S. Tsimring, and H. D. I. Abarbanel, *Phys. Rev. E* **51**, 980 (1995); H. D. I. Abarbanel, N. F. Rulkov, and M. M. Sushchik, *Phys. Rev. E* **53**, 4528 (1996).  
<sup>7</sup>J. F. Heagy, T. L. Carroll, and L. M. Pecora, *Phys. Rev. E* **50**, 1874 (1994).  
<sup>8</sup>D. J. Gauthier and J. C. Bienfang, *Phys. Rev. Lett.* **77**, 1751 (1996).  
<sup>9</sup>G. Chen and X. Dong, *Int. J. Bifurcation Chaos* **3**, 1363 (1993).  
<sup>10</sup>R. He and P. G. Vaidya, *Phys. Rev. A* **46**, 7387 (1992).  
<sup>11</sup>H. M. Rodrigues, ‘‘Uniform ultimate boundedness and synchronization,’’ preprint CDSNS94-160, Georgia Institute of Technology.  
<sup>12</sup>N. F. Rulkov, A. R. Volkovskii, A. Rodríguez-Lozano, E. del Río, and M. G. Velarde, *Int. J. Bifurcation Chaos* **2**, 669 (1992).  
<sup>13</sup>C. W. Wu, and L. O. Chua, *Int. J. Bifurcation Chaos* **4**, 979 (1994).  
<sup>14</sup>P. Ashwin, J. Buescu, and I. Stewart, *Phys. Lett. A* **193**, 126 (1994); *Nonlinearity* **9**, 703 (1996).  
<sup>15</sup>L. M. Pecora and T. L. Carroll, *Phys. Rev. Lett.* **64**, 821 (1990); *Phys. Rev. A* **44**, 2374 (1991).  
<sup>16</sup>M. de Sousa Vieira, A. L. Lichtenberg, and M. A. Lieberman, *Phys. Rev. A* **46**, R7359 (1992).  
<sup>17</sup>J. H. Peng, E. D. Ding, M. Ding, and W. Yang, *Phys. Rev. Lett.* **76**, 904 (1996).  
<sup>18</sup>D. M. Walker and A. I. Mees, ‘‘A nonlinear observer for synchronization of chaotic systems,’’ preprint CADO, Department of Mathematics, University of Western Australia, Nedlands WA 6907 (1996).  
<sup>19</sup>N. F. Rulkov, A. R. Volkovskii, A. Rodríguez-Lozano, E. del Río, and M. G. Velarde, *Chaos Solitons Fractals* **4**, 201 (1994).  
<sup>20</sup>J. F. Heagy, T. L. Carroll, and L. M. Pecora, *Phys. Rev. E* **52**, R1253 (1995).  
<sup>21</sup>E. Ott and J. C. Sommerer, *Phys. Lett. A* **188**, 39 (1994).  
<sup>22</sup>N. Gupte and R. E. Amritkar, *Phys. Rev. E* **48**, R1620 (1993).  
<sup>23</sup>M. -Z. Ding and E. Ott, *Phys. Rev. E* **49**, R945 (1994).  
<sup>24</sup>T. C. Newell, P. M. Alsing, A. Gavrielides, and V. Kovanis, *Phys. Rev. E* **49**, 313 (1994).  
<sup>25</sup>N. F. Rulkov and A. R. Volkovskii, *Proc. SPIE* **2038**, 132 (1993).  
<sup>26</sup>F. Verhulst, *Nonlinear Differential Equations and Dynamical Systems* (Springer-Verlag, Berlin, 1990).  
<sup>27</sup>G. H. Golub and C. F. Van Loan, *Matrix Computations*, 2nd ed. (Johns Hopkins University Press, Baltimore, 1989).  
<sup>28</sup>B. R. Hunt and E. Ott, *Phys. Rev. Lett.* **76**, 2254 (1996).  
<sup>29</sup>P. Cvitanović, *Physica D* **83**, 109 (1995); R. Artuso, E. Aurell, and P. Cvitanović, *Nonlinearity* **3**, 325 (1990); 361 (1990).  
<sup>30</sup>W. H. Press, S. A. Teukolski, W. T. Vetterling, and B. P. Flannery, *Numerical Recipes in C*, 2nd ed. (Cambridge University Press, New York, 1992).  
<sup>31</sup>W. L. Brogan, *Modern Control Theory*, 3rd ed. (Prentice-Hall, Englewood Cliffs, NJ, 1991).  
<sup>32</sup>A. R. Volkovskii and N. F. Rulkov, *Tech. Phys. Lett.* **71**, 65 (1993).  
<sup>33</sup>L. Kocarev and U. Parlitz, *Phys. Rev. Lett.* **76**, 1816 (1996).  
<sup>34</sup>Y.-C. Lai and C. Grebogi, *Phys. Rev. E* **52**, R3313 (1995).  
<sup>35</sup>N. Platt, E. A. Spiegel, and C. Tresser, *Phys. Rev. Lett.* **70**, 279 (1993).  
<sup>36</sup>S. C. Venkataramani, T. M. Antonsen, E. Ott, and J. C. Sommerer, *Phys. Lett. A* **207**, 173 (1995).  
<sup>37</sup>C. R. Wylie and L. C. Barrett, *Advanced Engineering Mathematics*, 6th ed. (McGraw-Hill, New York, 1995).  
<sup>38</sup>Y.-C. Lai and C. Grebogi, *Phys. Rev. E* **47**, 2357 (1993).  
<sup>39</sup>M. Di Bernardo, *Int. J. Bifurcation Chaos* **6**, 557 (1996).  
<sup>40</sup>E. D. Sontag, *Mathematical Control Theory* (Springer-Verlag, New York, 1991).